Probabilistic seismic demand model and optimal intensity measures for mid-rise steel modular building systems (MBS) under near-field ground motions

Ali Bigdeli [a], Amirhossein Emamikoupaei [b], Konstantinos Daniel Tsavdaridis [c],[*]

[a] Department of Civil and Environmental Engineering, Tarbiat Modares University, Tehran, Iran
[b] Department of Civil and Environmental Engineering, Shahid Beheshti University, Tehran, Iran
[c] Department of Engineering, School of Science & Technology, City, University of London, Northampton Square, EC1V 0HB, London, UK

ARTICLE INFO

ABSTRACT

Establishing suitable probabilistic seismic demand models (PSDMs) is a key part of the probabilistic performance-based method. Intensity measures (IMs) are used as a connection between earthquake hazard and seismic response in performance-based earthquake engineering. This study identifies the optimal intensity measures (IMs) of probabilistic seismic demand models for steel Modular Building Systems (MBSs) subjected to near-field earthquake ground motions. It is achieved by performing a Cloud analysis utilizing two sets of near-field ground motions: 72 pulse-like and 120 non-pulse-like ground motions. The nonlinear time history analysis is carried out using a finite-element model of a 6-story mid-rise MBS. For this aim, a total of 36 scalar intensity measures were collected. Based on a large number of regression analyses between the IMs and Engineering Demand Parameters for the studied MBS, the selected IMs were evaluated on several criteria, including correlation, efficiency, practicality, sufficiency, and proficiency. Finally, in the framework of PSDMs, different fragility curves and seismic demand hazard curves were generated for the studied MBS.

1. Introduction

Off-site modular prefabricated construction is an efficient, sustainable, and cost-effective method of construction. Modular units, as well as their interior components like studs, walls, ceilings, floors, etc., are transported and assembled on-site to form the total structure [1–4]. Typically, square hollow sections (HSS) and wide flange channels (W) are the sections used for columns and beams, respectively [5]. The key advantages of this form of the buildings are high quality, precise completion time forecasting, and reduced resource waste [6–8]. Consequently, modular volumetric buildings are becoming more popular in locations with high seismic risk and are being used in a variety of building types, including schools, housing, hospitals, and hotels [9,10]. However, one of the most significant issues that might affect the seismic performance of modular prefabricated buildings is the lack of specific standards and guidelines for design or compliance criteria [11,12].

In the framework of performance-based earthquake engineering (PBEE), seismic vulnerability is addressed by developing fragility curves that depict the conditional probability of the structure exceeding a certain limit state given the intensity measure (IM) of the ground motion [13]. Thus, one of the essential criteria for reliable fragility and probabilistic seismic demand analyses is the selection of

appropriate IMs [14,15], while prior research has recognized the importance of this criterion [16]. IM, in particular, functions as a link between seismic hazard analyses and structural demand evaluations [17]. Before generating fragility curves, probabilistic seismic demand models should be used to establish the optimal IMs that correlate adequately with the resultant EDPs (PSDM). PSDM is a conditional representation of the probability that a structural component would experience demand for a given IM level [15]. Therefore, selecting the best IM is a critical task that aids in increasing confidence in PSDMs and subsequent risk assessments utilized in decision-making [18]. Although numerous studies have been conducted, no attempt has been made to assess the seismic vulnerability of MBSs under near-fault earthquakes.

Ground motions with near-fault directivity are not adequately represented in modern codes, and their impacts have not been sufficiently included in existing earthquake record prediction equations or probabilistic seismic hazard analysis methodologies. Due to the large pulse generated by these motions, structures may be subjected to one or two cycles of severe inelastic deformation, resulting in significant damage. Bertero et al. discovered the damaging potential of near-fault pulses [19]; however, it was not until the 1994 Northridge earthquake that the severe implications of near-fault ground motions on the performance of structures and the significance of incorporating their effects into the design process were recognized [20,21].

A considerable amount of research has been conducted on the identification of optimal intensity measures for structures. Heshmati and Jahangiri [22] investigated appropriate intensity measures (IMs) for estimating the response of four steel diagrid structures with 4, 8, 16, and 24 stories under strong earthquake ground motions. In this research, a set of 38 candidate IMs was considered, and their optimality for seismic demand estimation of the studied structures was determined using five criteria of efficiency, practicality, proficiency, sufficiency, and scaling robustness. It was concluded that seismic IM significantly impacts the structural response hazard of steel diagrid systems. In addition, it was derived that the appropriate IMs in terms of efficiency, practicality, proficiency, sufficiency, and scaling robustness for estimating seismic demands of the steel diagrid systems are PGV and PGV/PGA. The proposed IMs reduce the uncertainty in fragility curves. Haghgou et al. [23] studied optimal ground motion IM and plotting the structural fragility curve for an intake tower structure by considering the soil–water-tower interaction and material nonlinearity through probabilistic seismic demand analysis. IMs and EDPs were chosen and classified based on their specifications. The optimal probabilistic seismic demand model was then determined by evaluating the IM-EDP charts generated for 150 ground motion records on a logarithmic scale using the goodness of fit, practicality, efficiency, proficiency, and sufficiency criteria. It was determined that the Cordova intensity has the greatest impact on the structural response of intake towers and better reveals the general trends of damage and failure. Huang et al. [17] identified optimal IMs for use in probabilistic seismic demand models (PSDMs) for circular tunnels in soft soil deposits. In this study, 18 IMs were selected employing correlation, efficiency, practicality, and proficiency criteria. The results showed that the peak ground acceleration (PGA) at the ground surface can be considered as the optimal IM for the shallow tunnels, whereas the peak ground velocity (PGV) can be considered as the optimal IM for both the moderately deep and deep tunnels. Wei et al. [24] evaluated the optimal IMs and seismic fragility of a multi-pylon cable-stayed bridge with super-high piers in mountainous areas. 16 ground motion IMs were utilized to assess the seismic performance of the multi-pylon cable-stayed bridge. The best IM was identified based on the practicality, efficiency, proficiency, sufficiency and hazard computability.

Several criteria have been proposed for determining the appropriate seismic IMs for structural evaluation, including efficiency, practicability, proficiency, sufficiency, and hazard calculability [14,15,25,26]. To date, these assessment measures and associated efforts have concentrated on structures [22,27,28], bridges [29], hydraulic structures [23,30,31], transmission towers [32] and, tunnels [17]. To the authors' knowledge, no relevant work dealing with steel modular building systems has been presented in the literature so far. A study conducted on the seismic performance of modular buildings indicates the necessity of investigating MBSs under near-field ground motions [33]. So it is crucial to find optimal IMs in order to develop the PBEE for these type of structures subjected to near-field records.

The objective of this paper is to identify the optimal IM of PSDMs and seismic vulnerability assessment of MBSs subjected to near-fault earthquake ground motions. For this purpose, 72 near-field forward-directivity (FD) and 120 near-field non-forward-directivity (NFD) earthquake ground motions records are considered in the context of a cloud analysis to obtain a wide range of response results. A six-story modular steel braced frame is chosen as a case study representing mid-rise MBSs. These ground motions are applied to the MBS using the finite element method. Then, the most optimal IMs for PSDMs of the MBS model for different engineering demand parameters (EDPs) are selected through five criteria: best correlation, efficiency, practicality, proficiency, and sufficiency. Finally, a seismic fragility curve for the MBS is built separately under the FD and NFD ground motions to determine its seismic vulnerability.

2. Earthquake ground motions

2.1. Near fault ground motion characteristics

Earthquake ground motions recorded at close site-to-source distances frequently exhibit significantly different features than those recorded at further distances; they may include velocity pulses caused by the forward direction of the earthquake (rupture toward the site). As a result, near-fault records are divided into "pulse-like"(contains forward directivity effect) and "non-pulse-like"(without forward directivity effect) categories. Ground motion records with a forward directivity effect typically produce powerful, double-sided pulses that occur early in the velocity-time series. These high-velocity pulse motions can have a significant effect on a structure's seismic performance [34,35]. Apart from exceeding typical peak ground velocity (PGV) values, the period of the velocity pulse (T_P) with respect to the structure's fundamental period (T) is essential for seismic behavior [34]. However, depending on the fault orientation and rupture propagation, backward- and neutral-directivity may exist [36].

The seismic energy released during fault rupture accumulates as the rupture velocity is slightly slower than the shear wave velocity [37,38]. This produces a strong double-sided pulse that often arrives early in the velocity time series at the recording site. The opposite

is observed behind pulse propagation in the backward directivity zone, and recordings often have long durations but small amplitudes. On strike-slip and dip-slip faults, FD effect can occur. FD typically affects sites located in the direction of fault rupture and near the end of a strike-slip fault. For dip-slip faults, FD has the greatest effect on locations located up dip of the rupture plane. A second near-fault phenomenon that might affect recordings and result in a pulse in the velocity time series is fling-step. This phenomenon is produced by the site's permanent ground displacement.

pulse-like near-fault earthquakes are often believed to be more destructive for long-period structures, e.g., tall buildings and isolated systems. However, Previous research [39] about the behavior of buildings to pulse-like behavior indicates that acceleration and drift demands on buildings are highly dependent on the ratio between the fundamental period of the system and the pulse characteristic period. Specifically if this ratio ranges between 2/3 and 1, both drift demands and top floor accelerations can be twice what is observed for buildings with fundamental periods that are 1.5 times the pulse characteristic period. Hence the critical parameter to consider is the ratio of the fundamental period of the structure to the pulse characteristic period. Mavroeidis and Papageorgiou (2003), provides a formula for the median value of the latter [40]:

$$T_p = 10^{(0.5Mw-2.9)} \tag{1}$$

Consequently, a moderate earthquake (Mw = 5.5) would lead to a characteristic period of 0.7 s. Taking that into account, buildings with a fundamental period ranging between 0.45 and 0.7 could be subjected to enhanced drift and acceleration demands if compared to buildings with larger fundamental periods (i.e. 1s). Therefore, moderately-tall modular buildings could be severely impacted instead.

The assessment that near-fault pulse-like ground motion affects more buildings with long periods is a product of the larger news coverage of large magnitude events, which have larger characteristic periods (for example, a Moment magnitude of 6 instead of 5.5 would end with a characteristic period of 1.26 s) which lead to extensive damage in longer period structures. However, it is clear that the occurrence of moderate and low magnitude events is more likely than higher magnitude events, thus, risk (defined at the expected value of the annual loss) is indeed larger for mid-rise structures.

2.2. Selecting records

This paper aims to find the optimum IMs for developing PSDMs for mid-rise modular steel structures. Ground motion selection is critical for seismic vulnerability assessment of structural components or systems. A significant number of ground motions must be examined to account for uncertainties during the ground motion selection process. To this goal, a group of 72 unscaled pulse-like near-fault ground motions (forward-directivity, FD) is picked using Baker's database [41]. In addition, 120 non-pulse-like near-fault ground motions (non-forward directivity, NFD) were utilized to compare the pulse-like record set to the non-pulse-like record set. Ground motion data is derived from the PEER database [42]. This expanded range of ground motions enables the model to exhibit various behaviors, from elastic response to failure. The non-pulse-like NFD records are chosen based on two criteria: (1) fault distance less than 20 km and (2) PGV/PGA ratio greater than 0.1. These FD and NFD earthquake records are based on data from events with a magnitude of 5 < M < 9 and various soil types. The acceleration response spectra of all chosen recordings are displayed in Fig. 1, together with their mean. Different ways of examining the relationship between a numerically anticipated engineering demand parameter (EDP) and a specified seismic IM may be found in the literature. However, This study uses cloud analysis since, contrary to far-field ground motions, near-fault ground motions cannot be fully captured using simple uniform scaling [43]. Cloud analysis is a numerical process that involves subjecting a structure to a series of (unscaled or as-recorded) ground motions and then numerically analyzing them [31].
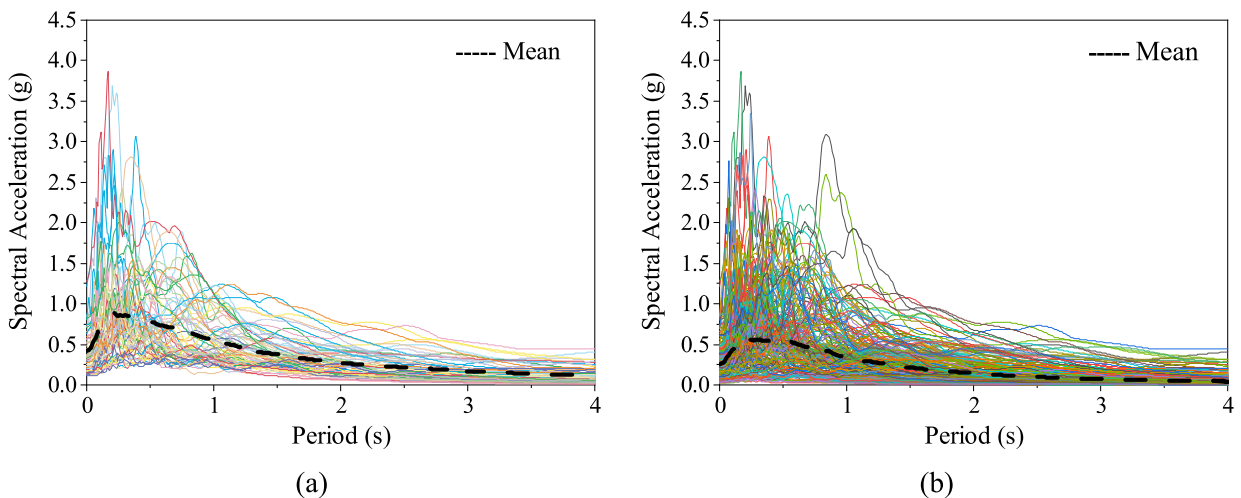

Fig. 1. Acceleration response spectra of all selected ground motions, considering 5% damping for: (a) FD records, (b) NFD records.

3. Seismic vulnerability assessment

The Pacific Earthquake Engineering Research Center (PEER) proposes a methodology for assessing seismic vulnerability [13]. This approach intends to compute the likelihood that an engineering demand parameter (EDP) would exceed various levels for a given design limit state at a certain ground motion intensity measure (IM). These can be employed in performance prediction to account for intrinsic randomness (a measure of our incapacity to interpret seismic and structural elements fully) and uncertainty (a measure of errors integrated into calculating models and procedures as a consequence of our inability). Eq. (2) mathematically defines the vulnerability assessment component of the PEER performance-based evaluation approach [44].

$$\lambda[LS] = \iint_{EDP,IM} P[LS|EDP] |dP[EDP|IM]| |d\lambda[IM]| \tag{2}$$

Where P [LS|EDP] represents the conditional probability of exceeding LS given the EDP value. P [EDP|IM] demonstrates the conditional probability of exceeding each EDP value given the ground motion intensity measurement (IM), and the hazard curve, λ[IM], represents the mean annual frequency of occurrence of earthquakes with intensities exceeding IM at a particular location. To produce P [EDP|IM], pairs of IMs and EDPs must be defined in order to use PSDMs. By analyzing the results of nonlinear time-history analyses of structural responses under earthquake IMs, the relationship between ground motion IM and structural response EDP can be established. The conditional mean and standard deviation of EDP given IM can be calculated using regression on the cloud of response data from unscaled ground motions.

3.1. Probabilistic seismic demand model (PSDM)

Probabilistic seismic demand analysis (PSDA), which combines probabilistic seismic hazard analysis (PSHA) with nonlinear structure analysis, generates a PSDM [45]. The engineering demand parameter (EDP) and the ground motion intensity measure are linked in PSDMs (IM). Cornell et al. (2002) demonstrated that conditional seismic demands can be modeled using a lognormal distribution [46], as shown in Eq. (3):

$$P[EDP \geq edp|IM] = 1 - \varphi\left(\frac{\ln(edp) - \ln(\eta_{EDP|IM})}{\beta_{EDP|IM}}\right) \tag{3}$$

where $\Phi(.)$ is the standard normal cumulative distribution function, $\eta_{EDP|IM}$ is the median value of EDP given IM, and $\beta_{EDP|IM}$ is the logarithmic standard deviation or dispersion of the EDP conditioned on the IM. $P[EDP \geq edp|IM]$ at various IM levels for certain EDP limit states generates fragility curves, indicating the usage of PSDMs in PBEE. Moreover, in Eq. (4), the relationship between demand and IM is stated in the power form:

$$\eta_{EDP|IM} = a(IM)^b \tag{4}$$

where a and b are constants parameters of the linear regression. Equation (3) can be translated further into lognormal space, as shown in Eq. (5):

$$\ln(\eta_{EDP|IM}) = b.\ln(IM) + \ln(a) \tag{5}$$

where ln (a) is the vertical intercept and b is the slope constant. The data for regression is generated utilizing a set of N ground motions and nonlinear time history analyses on the selected MBS models. The N demand quantities are then plotted against the IM to estimate the regression parameters and the dispersion term, as shown in Eq. (6):

$$\beta_{EDP\backslash IM} \cong \sqrt{\frac{\sum_{i=1}^{n} (in(edp_i) - in(\eta_{EDP\backslash IM}))^2}{n-2}} \tag{6}$$

where edp_i represents the ith realization of EDP from the nonlinear time history analysis, and n represents the number of analyses.

3.2. Engineering demand parameters (EDP)

The structural seismic response characteristics should be represented by engineering demand parameters (EDPs). The following parameters are considered as the key engineering demand parameters (EDPs) in this study. The maximum value of the peak inter-story drift ratio (drift normalized by story height) over all stories is called the Inter-story Drift Ratio (MIDR). The maximum Roof Drift Ratio (MRDR) is the ratio of peak lateral roof displacement (relative to the base) to building height. The maximum value of the peak ceiling absolute acceleration over all stories of superstructures is known as the Maximum Ceiling Acceleration (MCA). Different expressions for calculating inter-storey drift ratio have been proposed in the literature, such as the relative horizontal displacement of the ceiling beam and floor beam in the same storey over the storey height [47] or the displacements of two consecutive floor beams in modular units [48]. In this work, inter-story drift ratios of ceiling beam to floor beam (IDRCF) and floor beam to floor beam (IDRFF) were considered as EDPs. Future studies should also consider residual inter-storey drift, which is one of the important metrics for determining potential damage levels and resilience and has grown in interest among the community [49].

Compared to traditional (framed) structures, structural analysis and seismic responses are more challenging in modular buildings

due to the complex nature of structural components and connections [50]. As a result, the optimal IMs for constructing PSDMs should include large numbers of earthquake characteristics as possible, such as the amplitude, frequency content, and duration of the strong part of ground motion, among others. Table 1 lists a total number of 36 scalar intensity measures collected for this purpose. This set of IMs has been widely employed in investigating probabilistic seismic demand models for a variety of structures. There are three forms of IMs: event-based, earthquake-based (estimated directly from the time history of ground motions), and structure-based (IMs obtained from response spectra of ground motion time histories).

Table 1
Selected intensity measures (IMs) in this study.

Cat.		IM	Name	Definition	Unit	Ref.
Earthquake-based	1	PGA	Peak ground acc.	$\text{Max}\|\ddot{u}_g(t)\|$, $\ddot{u}_g(t)$ is acc. time history	cm/s²	–
	2	PGV	Peak ground vel.	$\text{Max}\|\dot{u}_g(t)\|$, $\dot{u}_g(t)$ is vel. time history	cm/s	–
	3	PGD	Peak ground dis.	$\text{Max}\|u_g(t)\|$, $u_g(t)$ is dis. time history	cm	–
	4	V_{max}/A_{max}	Velocity to acceleration ration	PGV/PGA	s	–
	5	A_{rms}	Root mean square of acc.	$\sqrt{\dfrac{1}{t_{smd}}\int_{t=0}^{t_{smd}}\ddot{u}_g^2(t)\,dt}$	cm/s²	–
	6	V_{rms}	Root mean square of vel.	$\sqrt{\dfrac{1}{t_{smd}}\int_{t=0}^{t_{smd}}\dot{u}_g^2(t)\,dt}$	cm/s	–
	7	D_{ms}	Root mean square of dis.	$\sqrt{\dfrac{1}{t_{smd}}\int_{t=0}^{t_{smd}}u_g^2(t)\,dt}$	cm	–
	8	I_a	Arias intensity	$\dfrac{\pi}{2g}\int_{t=0}^{t_t}\ddot{u}_g^2(t)\,dt$	m/s	[51]
	9	I_c	Characteristic intensity	$(A_{rms}^{1.5})(t_{smd}^{0.5})$	cm$^{1.5}$/s$^{2.5}$	[52]
	10	I_{cm}	Cosenza-Manfredi intensity	$\dfrac{2gI_A}{\pi(PGA)(PGV)}$	–	[53]
	11	SED	Specific energy density	$\int_{t=0}^{t_{smd}}\dot{u}_g^2(t)\,dt$	cm²/s	–
	12	CAV	Cumulative absolute vel.	$\int_{t=0}^{t_t}\|\ddot{u}_g(t)\|\,dt$	cm/s	[54]
	13	I_f	Fajfar intensity	$(PGV)(t_{smd}^{0.25})$	cm/s$^{0.75}$	[55]
	14	I_H	Housner intensity	$\int_{T=0.1}^{2.5}PS_v(T, \zeta = 5\%)\,dt$	cm	[56]
	15	EDA	Effective design acc.	Peak acc. After filtering out frequencies beyond 9 hz	cm/s²	[54]
	16	$A95$	A95 parameter	$0.764\,I_a^{0.438}$	cm/s²	[57]
	17	SMA	Sustained maximum acc.	3rd largest peak in $\ddot{u}_g(t)$	cm/s²	[58]
	18	SMV	Sustained maximum vel.	3rd largest peak in $\dot{u}_g(t)$	cm/s	[58]
	19	ASI	Acc. Spectrum intensity	$\int_{T=0.1}^{0.5}S_a(T, \zeta = 5\%)\,dt$	cm/s	[59]
	20	VSI	Vel. Spectrum intensity	$\int_{T=0.1}^{2.5}S_v(T, \zeta = 5\%)\,dt$	cm	[59]
Event - based	21	t_{smd}	Strong motion duration	$t_{0.95I_a}-t_{0.05I_a}$	s	–
	22	T_P	Predominant period	–	s	[60]
	23	T_M	Mean period	$\dfrac{\sum c_i^2/f_i}{c_i^2}$, c_i is the fourier amplitude, f_i is the discrete frequency corresponding to c_i	s	[61]
	24	M	Magnitude		Richter	–
	25	R	Site to source distance		km	–
	26	V_{S30}	Shear wave velocity		m/s	–
Structure-based	27	$S_a(T_1)$	Elastic spectral acc. at first period	$s_a(T_1, \zeta = 5\%)$	cm/s²	–
	28	$S_a(T_2)$	Elastic spectral acc. at second period	$s_a(T_2, \zeta = 5\%)$	cm/s²	–
	29	$S_a(T_3)$	Elastic spectral acc. at third period	$s_a(T_3, \zeta = 5\%)$	cm/s²	–
	30	$S_a(1.5T_1)$	Elastic spectral acc. at 1.5 time of the first period	$s_a(1.5\,T_1, \zeta = 5\%)$	cm/s²	–
	31	$S_a(2T_1)$	Elastic spectral acc. at 2 time of the first period	$s_a(2\,T_1, \zeta = 5\%)$	cm/s²	–
	32	$S_v(T_1)$	Elastic spectral vel.	$s_v(T_1, \zeta = 5\%)$	cm/s	–
	33	$S_d(T_1)$	Elastic spectral dis.	$s_d(T_1, \zeta = 5\%)$	cm	–
	34	s_a^c	Cordova intensity	$S_a(T_1)\sqrt{\dfrac{S_a(2T_1)}{S_a(T_1)}}$	cm/s²	[62]
	35	s_a^{c*}	Modified cordova intensity	$S_a(T_1)\sqrt{\dfrac{S_a(1.5T_1)}{S_a(T_1)}}$	cm/s²	–
	36	s_a^{tp}	Two-period intensity	$[S_a(T_1)]^{\frac{M_1}{M_1 + M_2}}[S_a(T_2)]^{\frac{M_2}{M_1 + M_2}}$, M_i is effective mass of i th mode	cm/s²	[63]

4. Selection of optimal intensity measures (IMs)

It is important to define the criteria for choosing appropriate ground motion IMs. The relationship between the structural response and ground motion should be correctly reflected in an acceptable IM. The goal is to lessen the disparity between structural responses to various ground motions. As described in the literature [14,15,25], an ideal seismic IM must have several characteristics. Correlation testing, efficiency, practicality, proficiency, and sufficiency are all examined in this article.

4.1. Correlation testing

The correlation criteria reveal how well the linear regression model matches the seismic demand computed. The correlation co-efficient R^2 is a criterion that ranges from 0 to 1. A greater R^2 suggests that there is lower dispersion and that EDP and IM have a better correlation relationship. As this value approaches one, the correlation testing improves, meaning that linear regression can more exactly estimate the data trend. Eq. (7) is used to compute this coefficient.

$$R^2 = \left(\frac{\sum_{i=1}^{n}(x_i - \bar{x})(y_i - \bar{y})}{\sqrt{\sum_{i=1}^{n}(x_i - \bar{x})^2}\sqrt{\sum_{i=1}^{n}(y_i - \bar{y})^2}} \right)^2 \tag{7}$$

The IM and EDP values for each earthquake record are x_i and y_i, respectively. The corresponding values of these data on the fitted regression line are $\bar{x}$ and $\bar{y}$.

4.2. Efficiency

Efficiency is an essential characteristic of IMs because more efficient IMs can anticipate seismic demand more precisely, and therefore the amount of variance in estimated structural demand for a given IM value is minimized when using an efficient IM. A more efficient IM requires fewer nonlinear time history analyses and, as a result, fewer earthquake records [26]. An effective IM can minimize variation in the predicted demand median indicated in equation (5) by the lower regression parameter $\beta_{EDP|IM}$.

4.3. Practicality

The concept of practicality examines the relationship between the demands imposed on the structure and the intensity measures of ground motions. The type of regression relationship used to obtain the median EDP for a particular IM determines the parameter necessary to quantify practicality. The practicability for a specific intensity measure is not strong, indicating that the change in this parameter has little impact on the seismic response of the engineering structure. Practicality is measured using the regression parameter b in Eq. (5) [15]. As b approaches zero, the IM's contribution to predicting the building's median response reduces. As a result, the higher the value of b, the more the EDP's reliance on the IM, and hence the more practical the IM.

4.4. Sufficiency

An alternative measure for selecting an optimal IM of PSDMs is sufficiency [25]. A sufficient IM leads the structural response to be conditionally independent of the earthquake magnitude, M, and the source-to-site distance, R, and to be dependent on the IMs [64]. A statistically significant p-value is typically used to determine sufficiency. A regression analysis of the residual $\varepsilon_{i|IM}$ and the ground motion parameters produces the p-value, where $\varepsilon_{i|IM}$ is the relative error between the real value of seismic response in each analysis and the estimated earthquake demand derived by the probabilistic seismic demand model (PSDM). The regression analysis p-value would be less than the stated significance threshold, suggesting that IM_i is insufficient. The criterion for an inadequate IM_i in this study was set at a p-value of 0.05. A higher p-value in the regression analysis indicates a sufficient IM.

4.5. Proficiency

Proficiency is another metric for evaluating the applicability of IMs in the PBEE introduced by Padgett et al. [10] to take into account both practicality and efficiency, balanced by Eq. (8). The typical method of selecting an ideal IM based on practicality and efficiency can result in balancing the two characteristics difficult. Proficiency combines practicality with efficiency to address the challenge. The lower the value of ζ, the greater the IM's proficiency.

$$\zeta = \frac{\beta_{EDP|IM}}{b} \tag{8}$$

4.6. Hazard computability

The hazard computability of a candidate IM is another criterion for judging its suitability. The level of effort required to calculate the hazard curve for an IM or assess seismic hazard probabilistically is referred to as hazard computability [14]. IM connects structural demands and seismic hazards in a region, as illustrated in Eq. (2). Accordingly, the probabilistic seismic hazard must be calculated using values dictated by the IM. While PGAs and spectral accelerations are available from hazard maps, other structure-dependent IMs require even more effort, and it can be difficult to calculate some of them from hazard maps.

5. Case study model

As a study case, a six-story steel MBS braced frame with five bays in each direction, and each story height of 3 m is developed in

accordance with AISC [65]. The MBS consists of five bay in each direction. Each module's dimensions are 6 m× 3.5 m ×3 m (length × width ×height). Fig. 2 depicts the 3D view of the studied MBS. The optimal frame sections for the MBS's columns, beams, and braces are detailed in Table 2. All columns, beams, and braces are made of square hollow sections (HSS), which are extensively utilized in MBSconstructions. Each module is modeled with horizontal axis gaps of 350 mm and vertical axes gaps of 200 mm, as illustrated in Fig. 3(a), to account for the center-line offset of columns and the small space between consecutive columns. The selected sections were given identical mechanical properties, such as modulus of elasticity = 200 GPa, yield strength = 350 MPa, and Poisson's ratio = 0.3.

Table 3 provides the superimposed dead load utilized for additional loads such as the floor, roof, corridor, and ceiling, as well as the live loads and the snow load used for the design. The earthquake design force is computed using ASCE07, taking into account the following parameters: importance factor Ie = 1 (Risk Category II for residential buildings), Site Class D (stiff soil), and response modification factor R = 6. The structure is assumed to be in California.

This study considers only the MBS's lateral response in the longitudinal direction. The system resisting lateral forces in this direction consists of two exterior X-braced frames. The braces are connected to the floor beam-to-column and ceiling beam-to-column joints in each story level in these frames. The brace connections to the modular frame system consist of gusset plates that are welded to the braces.

In order to conduct nonlinear dynamic analysis, a two-dimensional model of the MBS is created using the OpenSees software, as illustrated in Fig. 3. Nonlinearities in both materials and geometry are taken into account. The material used for the steel member is Grade 350 steel, which has a yield strength of 350 MPa and ultimate strength of 450 MPa. The elasticity modulus of this material is 200 GPa.

For evaluating the seismic response of SCBFs, the created models incorporate the nonlinear behavior associated with brace yielding in tension and the buckling/post-buckling behavior. In addition to any yielding of the beams and columns in the connection regions, the models took into account the deformation and yielding of gusset plate connections. Simplified discrete component models, such as beam-column elements and concentrated springs, were employed in the OpenSees model. Many of the modeling components were based on what Hsiao et al. had applied [66].

The uniaxial material Steel02 option in OpenSees defines the stress-strain relationship of this material. The element *force-BeamColumn* option in OpenSees is used to represent beam and column elements with fiber sections and five integration points per element. Brace elements are also modeled with the element *dispBeamColumn* option, including fiber sections and three integration points per element. The P-delta effect is taken into account as a source of geometric nonlinearity in the analysis. Braces are discretized using eight elements between work points, each having three integration points and an initial out-of-plan imperfection of L/500. To adequately capture the out-of-plane rotational behavior of gusset plates at the connections, single and multiple springs aligned with the brace and located at the ends were considered. As Hsiao et al. [66]demonstrated, a correct estimate for the gusset plate stiffness is critical for accurately capturing the buckling capacity of a brace. Zero-length nonlinear spring elements in OpenSees were used for welded connections, allowing strength and stiffness degradation simulation.

To account for damping, a Rayleigh damping ratio of 5% is assigned to the first and second modes of vibration in the nonlinear dynamic analysis. The nonlinear time history analysis is carried out using a step-by-step numerical integration method in which the parameters γ and β are assumed to be 0.5 and 0.25, respectively. When analyzing nonlinear static and dynamic systems, there may be
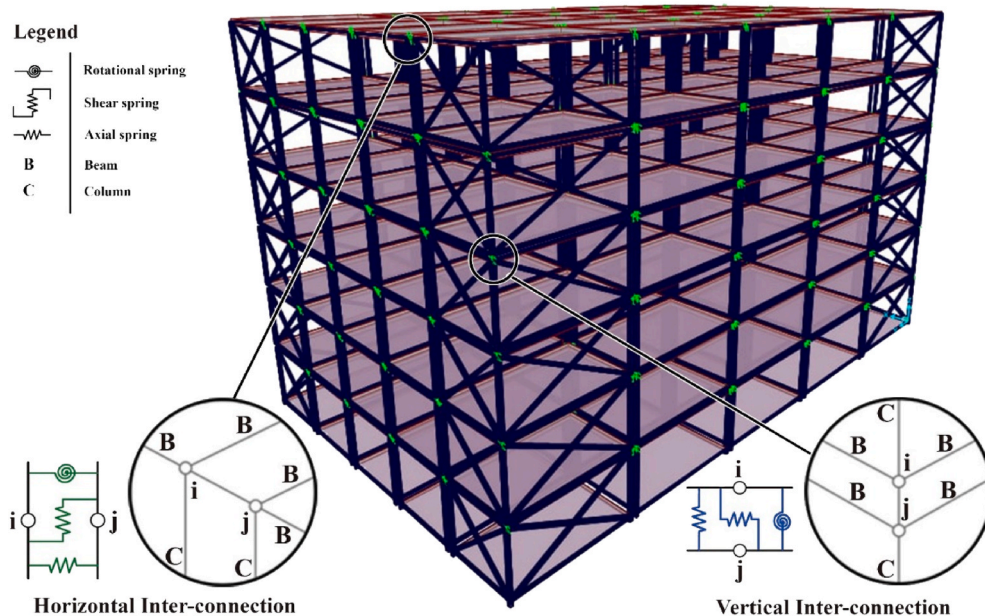

Fig. 2. 3D view of the case study with vertical and horizontal inter-module connection.

Table 2
Member section of studied MBS from seismic design.

6-story MBS			
Member	Story 1-2	Story 3-4	Story 5-6
Column	HSS 152×152×11.8	HSS 152×152×5.9	HSS 127×127×5.9
Floor beam	HSS 102×102×5.9	HSS 102×102×5.9	HSS 102×102×5.9
Ceiling beam	HSS 76×76×5.9	HSS 76×76×5.9	HSS 76×76×5.9
Brace	HSS 127×127×11.8	HSS 127×127×8.9	HSS 102×102×5.9

non-convergence problems. For this reason, it is necessary to define a solution algorithm object in order to ensure that the numerical solution is accurate. In order to solve the nonlinear equations, a sequence of steps is identified. Various algorithms are used to find non-convergent solutions.

For determining the ultimate lateral load resistance, nonlinear pushover analyses are conducted. An analysis of distributed plasticity is performed using OpenSees. Based on the combined behavior of inelastic materials and distributed plastic hinges along the elements, Fig. 4 illustrates the pushover (capacity) curve of the MBS. First, the gravity loads are applied in ten steps. Following this, the lateral loads of the structure are incrementally distributed along its height.

6. Results and discussions

The PSDMs are created by first performing nonlinear time history analyses on chosen unscaled FD and NFD data (Cloud analysis). The weaker axis of the mid-rise MBS is subjected to the horizontal component of earthquake ground motions. PSDM is formed by selecting four EDPs to assess the appropriateness of IMs in terms of correlation, efficiency, practicality, sufficiency, and proficiency. Fig. 5 shows the PSDM results from the maximum roof drift ratio MRDR as EDP plotted against PGV as IM in both arithmetic and logarithmic scales. Despite the fact that FD records have higher IM values, in the same value of IM, seismic responses of MBS under NFD records are higher than in FD records. As the regression line for NFD records is located above the regression line for FD records, it can be concluded that the response of MBS may not be controlled by the pulse effect alone and that other features of near-field records also have their own impacts.

In order to further study the differences between FD and NFD records, a cloud of data of MRDR versus ln [PGA] is plotted in Fig. 6 by taking into account all records as near-field ground motion responses and classifying them as FD and NFD responses. It is evident that considering all data as response of near-field ground motions results in worse goodness of fitting and slope value than separating data as response subjected to FD and NFD ground motion records. When data are separated, there is an increase in both the goodness of fitting (R^2) and the slope of the regression line for NFD, while there is a drop in both R^2 and the slope of the regression line for FD records. It seems that pulse nature results in the seismic scattering response of MBS. Therefore, it is necessary to examine the response parameters independently.

The ratio of the pulse period to the fundamental period of the structure, T_p/T_1, is an essential characteristic of pulse-like motions that influences structural response. In Fig. 7, the MBS model response data under the FD records is shown against the ratio T_p/T_1. The pulse periods of selected FD ground motions in this study vary from 0.58 to 13.31 s. As the model's first period is 0.84 s, the T_p/T_1 ratio ranges between 0.7 and 15.84. A local average utilizing the Nadaraya-Watson kernel-weighted average with a Gaussian weight function is used to reflect the data's local variation [67]. Moreover, the means and medians of the NFD responses are shown; the mean response is greater than the median, indicating a bias toward higher values. The FD motions' response may be higher or lower than the NFD records' average response. Lower response values are seen mainly for MRDR when the ratio of T_p/T_1 rises. This trend can be seen in the IDRCF and IDRFF but is less evident in the MCA. Most records in IDRCF that exceed the drift limit (0.02) have a $T_p/T_1 < 2.5$ ratio. In IDRFF, however, this ratio is $T_p/T_1 < 14.25$.

6.1. Correlation testing

The correlation criteria, as previously stated, reveal how well the regression model of Eq. (5) matches the computed EDP. The correlation coefficient or goodness of fitting R^2 is the name for this criteria. In order to test the correlation between the examined IMs, linear regression was applied to the natural logarithm of the IM and EDP (i.e., Eq. (5)). As an example, regression analyses for four selected IMs, as listed in Table 1, are plotted in Fig. 8. The regressions refer to the MRDR results obtained from FD and NFD records as EDP against IMs, namely Arias intensity, S_a^{tp}, VSI, and $S_a(T_1,\zeta)$. Table 4 and Table 5 summarize all regression parameters estimated for the examined IMs under FD and NFD ground motions for the mid-rise MBS, respectively.

The goodness of fitting R^2 values of logarithmic linear trend lines in Tables 4 and 5 are independently presented in Figs. 9–12 for selected EDPs to evaluate the correlation of the obtained IM-EDP pairs. When comparing R^2 values for FD and NFD data, it can be shown that R^2 values for NFD records are considerably higher than FD records in structure-based and earthquake categories, notably in IMs vs. MCA. In the event-based category, however, the opposite trend is observed.

Fig. 9 illustrates the correlation coefficient of MRDR against IMs. As it is observed, IM = modified Cordova intensity (S_a^c*) would result in $R^2 = 0.860$ value, and it better correlates with MRDR under the FD records. Two-period intensity (S_a^{tp}) with R^2 values of 0.835 and $S_a(T_1,\zeta)$ together with $S_v(T_1,\zeta)$ with the R^2 value of 0.831 for both IMs show the second and third-strongest correlations with MRDR. Besides, VSI with the R^2 value of 0.815 is a good alternative. The first three highest R^2 values under NFD records belong to S_a^{tp} With $R^2 = 0.980$, followed by $S_a(T_1,\zeta)$, $S_v(T_1,\zeta)$, and $S_d(T_1,\zeta)$, all with the correlation of coefficient of 0.979 and VSI with $R^2 = 0.922$.
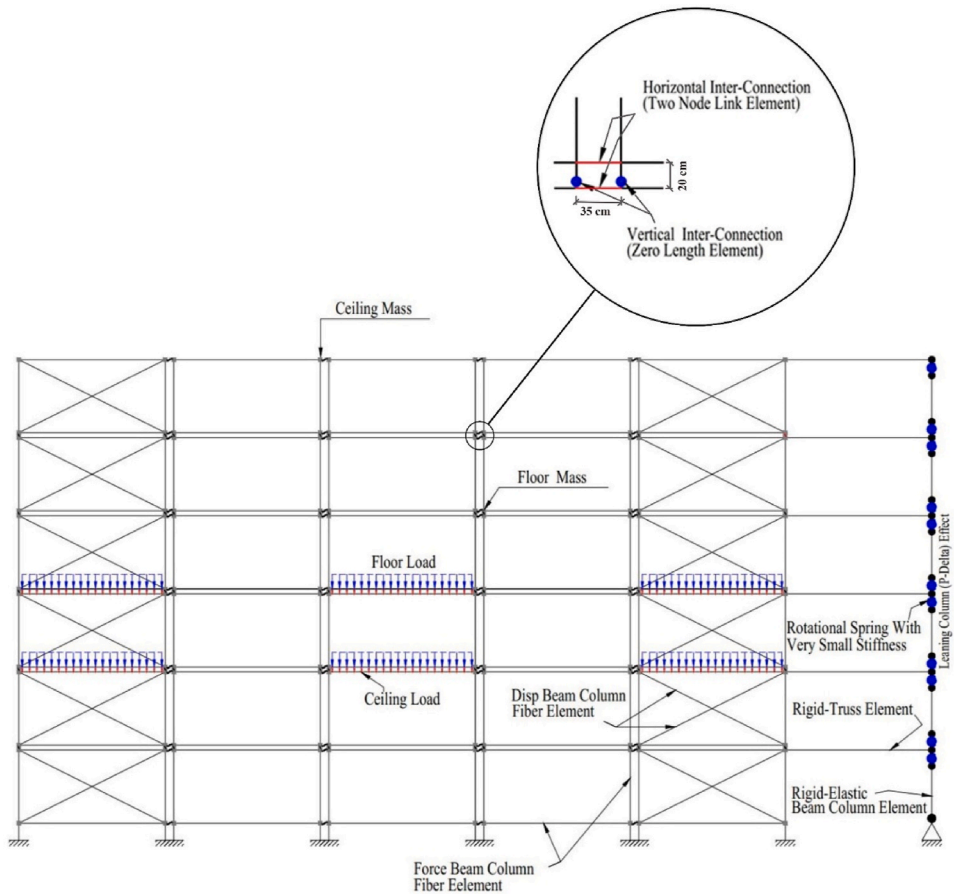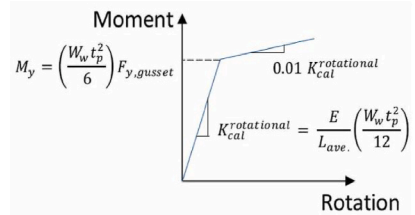
(a)
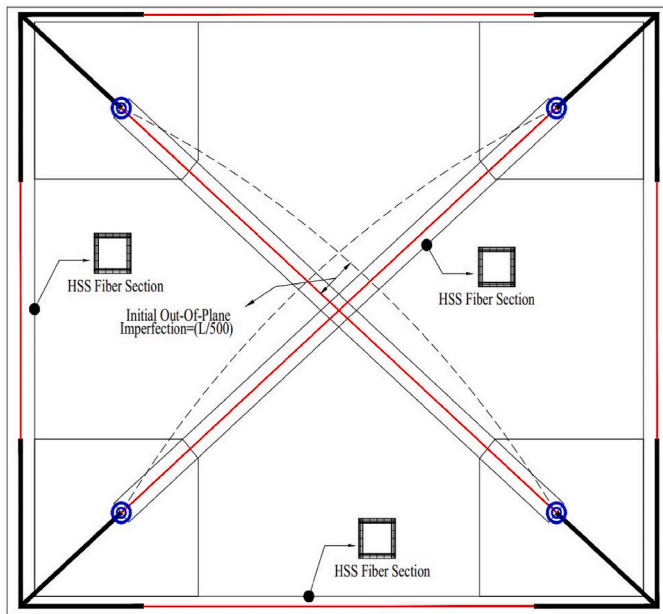
(b)

(caption on next page)

Fig. 3. Details of modeling the MBS in OpenSees (a) two-dimension model (b) schematic view of brace modeling.

Table 3
Superimposed dead, live and snow load applied for the design of MBS.

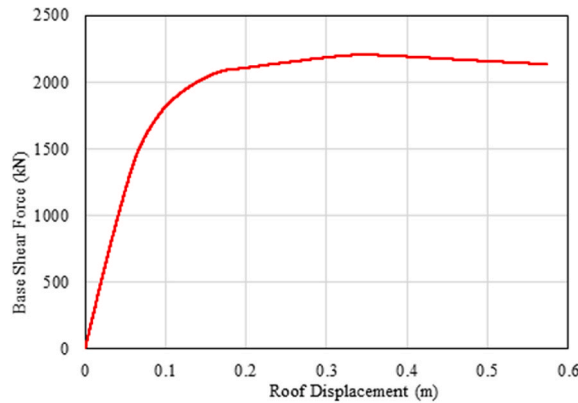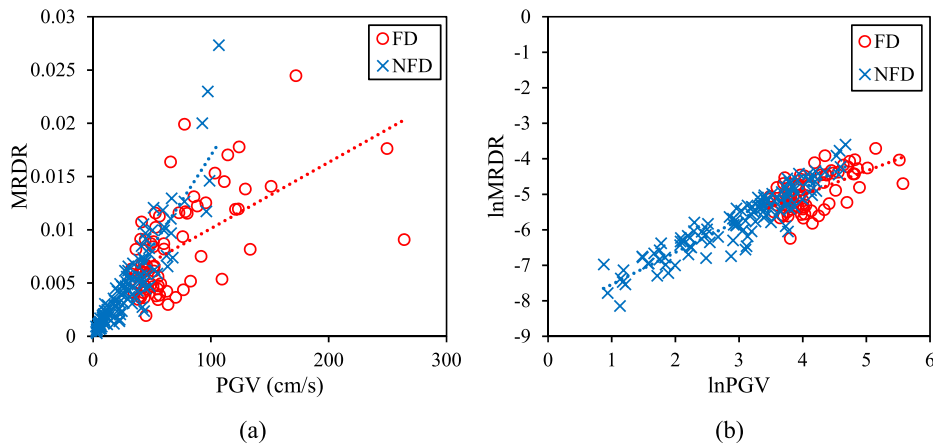| Structural components	Load type	Load
Floor slab	Superimposed dead load	0.75 KN/m^2
	Live load	2 KN/m^2
Ceiling slab	Superimposed dead load	0.7 KN/m^2
Roof	Superimposed dead load	0.32 KN/m^2
	Live load	1 KN/m^2
	Snow load	1 KN/m^2
Corridor	Live load	4.8 KN/m^2
External Floor beam	Dead load	1.5 kN/m

Fig. 4. Pushover curve of the studied MBS.

Fig. 5. Results of cloud analysis in (a) arithmetic (b) logarithmic scale.

However, PGD, D_{rms}, and T_M with the goodness of fitting of 0.002, 0.007, and 0.010 subjected to FD records, and V_{max}/A_{max}, T_M, and V_{s30} with R^2 values of 0.001, 0.004, and 0.005 subjected to NFD ground motions have the weakest correlation.

Taking into account IDRCF as EDP (Fig. 10), the first three strongest correlations under FD records are modified Cordova intensity (S_a^c*), VSI and Two-period intensity (S_a^{tp}) with R^2 values of 0.788, 0.786 and 0.764, respectively. It is important to note that the elastic spectral acceleration, velocity, and displacement at the first period with all R^2 values of 0.758 are the next optimal IM. For NFD records, S_a^{tp} with $R^2 = 0.968$ has the strongest correlation with MRDR, followed by $S_a(T_1,\zeta)$ and $S_v(T_1,\zeta)$ with the correlation coefficient of 0.967 for both IM. S_a^c, S_a^c* and VSI are the next optimal IMs based on correlation testing. On the contrary, the weakest correlation between IMs and MRDR under FD ground motions is PGD with the goodness of fitting of 0.003, followed by T_M and D_{rms} with the correlation coefficients of 0.0083 and 0.0084, respectively. The weakest IM-EDP (MRDR) pairs under NFD records are V_{max}/A_{max}, T_M,
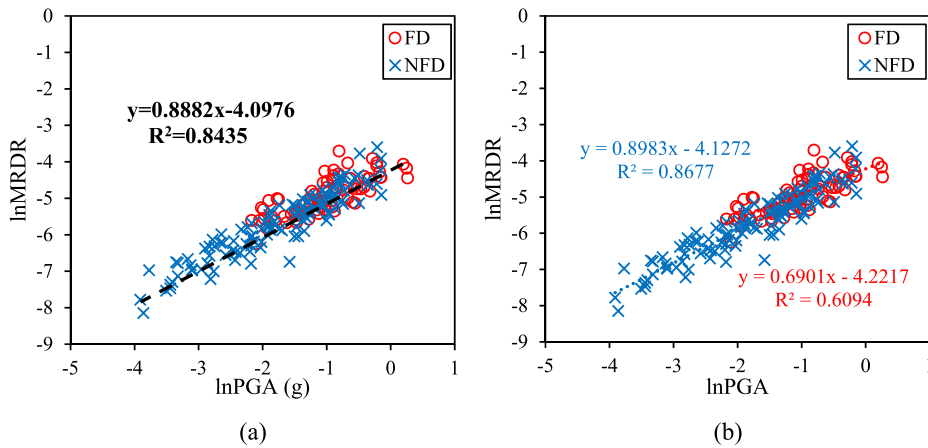
Fig. 6. Relationship between lnMRDR and lnPGA in (a) regression line for all of the data and (b) separate regression line for FD and NFD records.
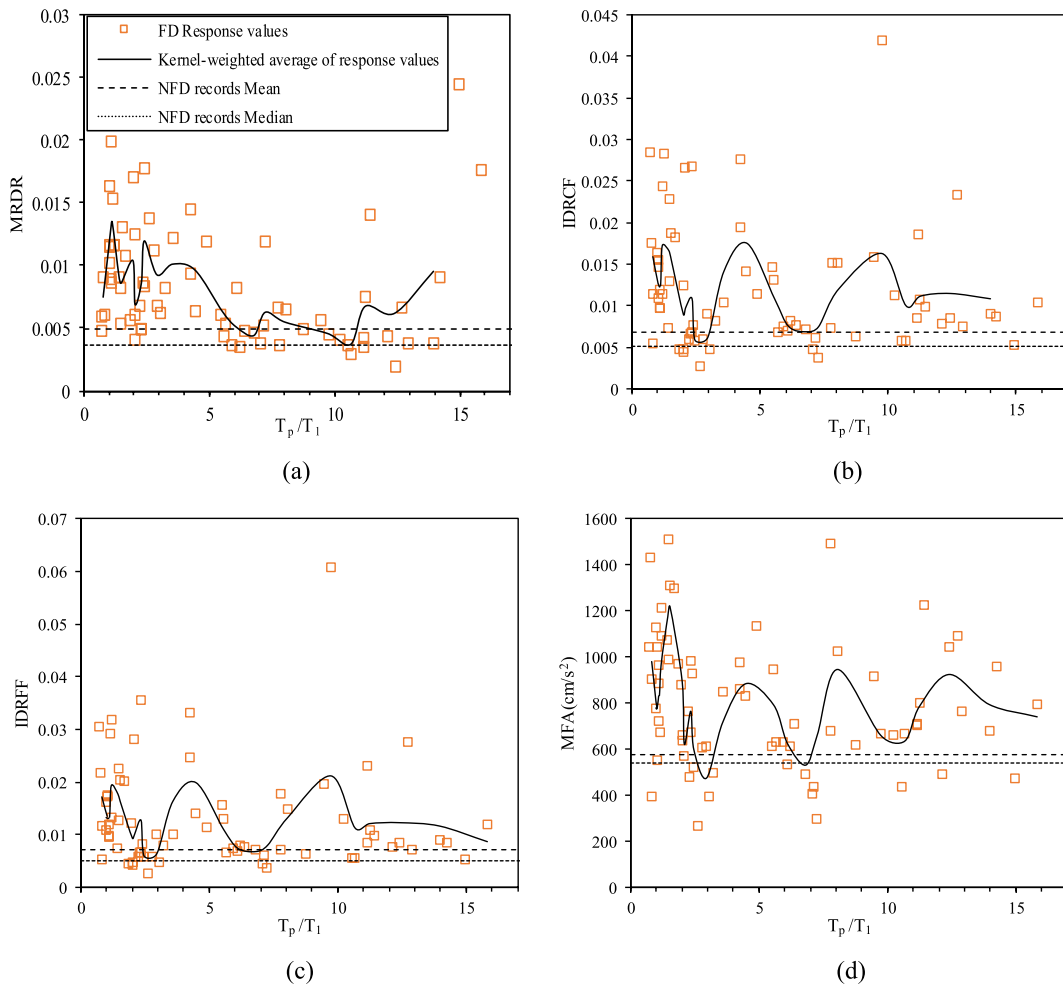
Fig. 7. Seismic response of MBS subjected to FD records in terms of T_p/T_1 (a) MRDR (b) IDRCF (c) IDRFF (d) MCA.

and V_{s30}, with R^2 values of 0.002, 0.004, and 0.009, respectively. The correlation coefficient for IDRFF against IMs is plotted in Fig. 11 for the FD and NFD records. The goodness of fitting R^2 Calculated for IDRFF and the trend of strongest and weakest IMs are similar to the results obtained from IDRCF,

Fig. 8. Regression analyses between four representative seismic IMs and MRDR.

Fig. 12 depicts the computed results of the correlation coefficients for MCA. It can be seen that under both FD and NFD records, the IMs that are related to acceleration have the highest R^2 value. IMs including ASI, $S_a(T_1,\zeta)$, and EDA strongly correlat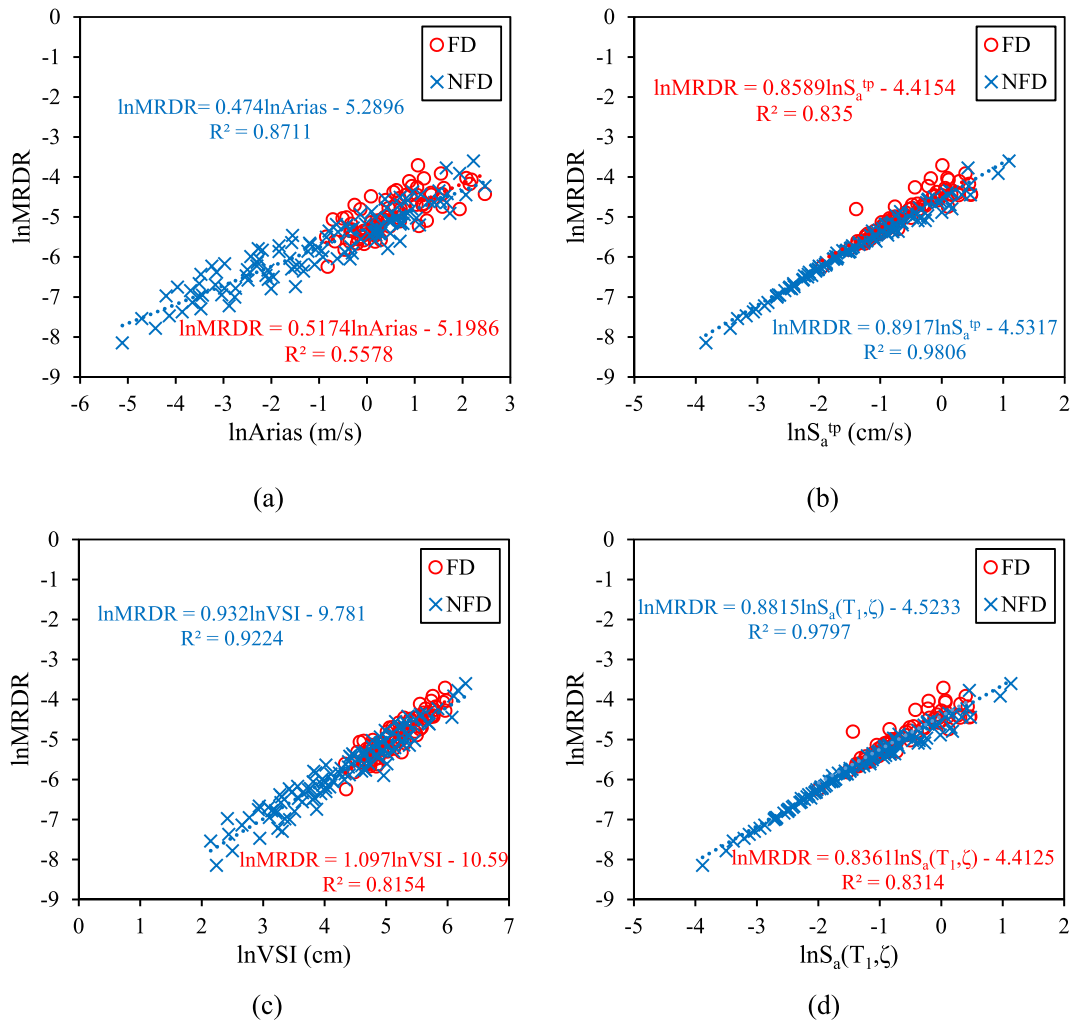e with MCA under FD and NFD records. These R^2 values are 0.793, 0.757 and 0.739, respectively under FD records and 0.935, 0.927 and 0.918, respectively under NFD records. Interestingly, under FD records, IMs that are related to the velocity have the weakest correlation with MCA. The first three weakest R^2 values for the MBS subjected to FD ground motions are 0.0007, 0.0009, and 0.003, corresponding to V_{rms}, I_f, and SMV, respectively. On the other hand, the weakest R^2 values under NFD records belong to V_{s30} ($R^2 \approx 0$), V_{max}/A_{max} ($R^2 = 0.019$) and T_p ($R^2 = 0.020$).

6.2. Efficiency criterion

As mentioned earlier, the efficiency of intensity measures can be assessed by comparing the standard deviation $\beta_{EDP|IM}$. In general, the smaller the conditional logarithmic standard deviation is for each IM_i, the smaller the discrete type of seismic response to structures is. This indicates that the ground motion parameter IM_i is more efficient.

By using the Cloud analysis method, the seismic response was calculated under FD and NFD earthquake ground motions and the conditional logarithmic standard deviation, $\beta_{EDP|IM}$, corresponding to the intensity measures, was extracted. The result of efficiency analysis is demonstrated in Figs. 13–16 for four selected EDPs. Under the FD ground motions, the value of $\beta_{EDP|IM}$ for most IMs related to the earthquake-based and structure-based is higher than NFD ground motions. However, in event-based IMs, the conditional logarithmic standard deviation for NFD records is significantly higher than for FD records. In general, NFD ground motions are more efficient at predicting the EDPs than FD motions; that is, regression models fit better to data from the NFD ground motion set than to data from FD.

According to Fig. 13, S_a^{c*}, S_a^{tp} and $S_{a,v,d}(T_1,\zeta)$ are considered more efficient measures for MRDR under FD ground motions since they have smaller standard deviations $\beta_{EDP|IM}$. The value of $\beta_{EDP|IM}$ for mentioned IMs are 0.20, 0.218 and 0.220, respectively. VSI with $\beta_{EDP|}$

Table 4
Regression parameters and goodness of fitting for MBS under FD records.

IM	Engineering Demand Parameters											
	MRDR			IDRCF			IDRFF			MCA		
	b	a	R^2	b	a	R^2	b	a	R^2	b	a	R^2
PGA	0.69	0.01	0.61	0.72	0.02	0.59	0.79	0.02	0.57	0.52	1273.61	0.72
PGV	0.68	0.00	0.36	0.70	0.00	0.34	0.83	0.00	0.38	0.19	343.58	0.06
PGD	−0.03	0.01	0.00	−0.03	0.01	0.00	−0.01	0.01	0.00	−0.13	1156.21	0.12
V_{max}/A_{max}	−0.28	0.00	0.10	−0.30	0.01	0.10	−0.29	0.01	0.08	−0.42	362.70	0.45
ACC RMS	0.73	0.07	0.51	0.75	0.10	0.48	0.82	0.14	0.46	0.56	4198.34	0.61
Vel RMS	0.33	0.00	0.10	0.32	0.00	0.09	0.41	0.00	0.12	−0.02	778.91	0.00
Dis RMS	−0.04	0.01	0.01	−0.05	0.01	0.01	−0.03	0.01	0.00	−0.11	914.42	0.11
Arias Int.	0.52	0.01	0.56	0.53	0.01	0.53	0.59	0.01	0.52	0.34	624.24	0.50
I_c	0.67	0.04	0.59	0.68	0.06	0.55	0.76	0.08	0.54	0.46	2551.57	0.59
SED	0.06	0.00	0.02	0.06	0.01	0.02	0.08	0.01	0.03	−0.07	1304.02	0.05
CAV	0.41	0.00	0.10	0.41	0.00	0.09	0.47	0.00	0.10	0.18	212.21	0.04
ASI	0.65	0.02	0.47	0.68	0.02	0.47	0.75	0.03	0.45	0.59	1552.88	0.79
VSI	1.10	0.00	0.82	1.14	0.00	0.79	1.29	0.00	0.80	0.52	49.68	0.38
Housner Int.	1.00	0.00	0.72	1.03	0.00	0.68	1.18	0.00	0.71	0.39	102.17	0.22
SMA	0.71	0.02	0.50	0.73	0.03	0.48	0.79	0.03	0.45	0.52	1529.31	0.56
SMV	0.14	0.00	0.03	0.20	0.00	0.05	0.24	0.00	0.06	0.03	660.73	0.00
EDA	0.74	0.02	0.64	0.77	0.02	0.62	0.85	0.03	0.60	0.55	1355.55	0.74
A95	0.69	0.01	0.61	0.71	0.02	0.59	0.79	0.02	0.57	0.52	1278.53	0.72
T_p	0.22	0.01	0.07	0.23	0.01	0.07	0.28	0.01	0.08	−0.11	669.27	0.03
T_m	−0.14	0.01	0.01	−0.13	0.01	0.01	−0.08	0.01	0.00	−0.54	629.61	0.34
I_f	0.40	0.00	0.14	0.42	0.00	0.14	0.51	0.00	0.16	0.02	667.62	0.00
I_{cm}	−0.66	0.00	0.22	−0.71	0.01	0.23	−0.84	0.01	0.26	−0.21	635.45	0.05
M	−2.06	0.39	0.12	−2.16	0.67	0.12	−2.16	0.70	0.09	−1.72	20861.46	0.17
R	−0.24	0.01	0.19	−0.24	0.02	0.18	−0.28	0.02	0.20	−0.10	885.80	0.08
t_{smd}	−0.34	0.02	0.24	−0.34	0.02	0.22	−0.38	0.03	0.22	−0.24	1334.76	0.25
V_{s30}	0.21	0.00	0.03	0.22	0.00	0.03	0.25	0.00	0.03	0.16	278.63	0.03
$S_a(T_1)$	0.84	0.01	0.83	0.84	0.02	0.76	0.94	0.02	0.76	0.41	963.05	0.42
$S_a(1.5T_1)$	0.82	0.02	0.67	0.83	0.02	0.62	0.95	0.03	0.64	0.26	958.46	0.14
$S_a(2T_1)$	0.59	0.02	0.36	0.61	0.02	0.34	0.72	0.03	0.38	0.13	879.87	0.04
$S_a(T_2)$	0.53	0.01	0.34	0.56	0.01	0.34	0.61	0.01	0.33	0.55	883.19	0.76
$S_a(T_3)$	0.51	0.01	0.40	0.53	0.01	0.40	0.58	0.01	0.38	0.47	898.21	0.72
$S_v(T_1)$	0.84	0.00	0.83	0.84	0.00	0.76	0.94	0.00	0.76	0.41	127.97	0.42
$S_d(T_1)$	0.84	0.00	0.83	0.84	0.00	0.76	0.94	0.00	0.76	0.41	294.53	0.42
Cor. Int.	0.97	0.02	0.77	0.98	0.03	0.72	1.12	0.03	0.74	0.38	1063.72	0.25
Mod. Cor. Int.	0.95	0.02	0.86	0.96	0.02	0.79	1.08	0.02	0.80	0.40	1018.26	0.31
Two period Int.	0.86	0.01	0.84	0.87	0.02	0.76	0.97	0.02	0.76	0.45	973.04	0.46

$_{IM}$ value of 0.230 is also another efficient IM. For NFD records, the first most efficient IM is S_a^{tp} ($\beta_{EDP|IM} = 0.126$). The next three most efficient IMs are $S_{a,v,d}(T_1,\zeta)$ with the $\beta_{EDP|IM}$ value of 0.129, S_a^c ($\beta_{EDP|IM} = 0.207$) and VSI ($\beta_{EDP|IM} = 0.252$). PGD has the highest standard deviation $\beta_{EDP|IM}$, which is 0.536, meaning it is the least efficient criterion in FD records. D_{rms} and I_M are the next two least efficient IM. Their $\beta_{EDP|IM}$ values are 0.535 and 0.534, respectively, which are marginally lower than the PGD standard deviation. The three least efficient IM against MRDR subjected to NFD records are V_{max}/A_{max}, T_M and V_{s30} with $\beta_{EDP|IM}$ value of 0.905, 0.904 and 0.903, respectively.

Under FD records, considering IDRCF as EDP, S_a^c* is the most efficient ground motion amplitude parameter (Fig. 14), followed by VSI and S_a^{tp} with $\beta_{EDP|IM}$ values of 0.260, 0.261, and 0.275, respectively. $S_{a,v,d}(T_1,\zeta)$ with the $\beta_{EDP|IM}$ value of 0.278 is also efficient IM. The least efficient IMs-IDRCF pair, on the other hand, is the same as MRDR, with $\beta_{EDP|IM}$ values of 0.565, 564, and 0.564, respectively. Under NFD ground motions, the first three most efficient predictors of the IDRCF are S_a^{tp}, $S_{a,v,d}(T_1,\zeta)$ and S_a^c (with $\beta_{EDP|IM}$ values of 0.163, 0.164 and 0.228, respectively). V_{max}/A_{max}, T_M, and V_{s30} have the lowest efficiency with $\beta_{EDP|IM}$ values of 0.917, 0.916, and 0.914, respectively. The results of the efficiency criterion analysis for IDRFF (Fig. 15), including the order of the most and the least efficient IMs, are the same as IDRCF. However, the fact that $\beta_{EDP|IM}$ for IDRFF is greater than IDRCF implies higher dispersion of IDRFF results.

The computed standard deviations $\beta_{EDP|IM}$ for MCA are plotted in Fig. 16. With the smallest standard deviation of 0.739, EDA is the most effective IM under FD records among the tested IMs, followed by $S_a(T_2,\zeta)$ and ASI with $\beta_{EDP|IM}$ of 0.757 and 0.793, respectively. It is found that V_{rms} with the standard deviation of 0.374 is the least efficient IM, followed by I_f and SMV. The standard deviation for each is 0.374 and 0.373, respectively. Establishing IM-MCA pairs under NFD ground motions reveals that ASI tends to be the most efficient, with the $\beta_{EDP|IM}$ value of 0.195. The two next efficient IMs are EDA and $S_a(T_2,\zeta)$. Their corresponding value of standard deviations is 0.208 and 0.220, respectively. However, IM=V_{s30} has the highest value of standard deviation ($\beta_{EDP|IM} = 0.772$), which means it is the least efficient IM when MBS is subjected to NFD records. The two latter least efficient IMs are V_{max}/A_{max} and T_p with $\beta_{EDP|IM}$ of 0.764 and 0.763, respectively.

Table 5

Regression parameters and goodness of fitting for MBS under NFD records.

IM	Engineering Demand Parameters											
	MRDR			IDRCF			IDRFF			MCA		
	b	a	R^2	b	a	R^2	b	a	R^2	b	A	R^2
PGA	0.90	0.02	0.87	0.91	0.02	0.86	0.93	0.02	0.86	0.79	1766.99	0.92
PGV	0.90	0.00	0.86	0.91	0.00	0.85	0.93	0.00	0.85	0.77	43.23	0.86
PGD	0.58	0.00	0.50	0.58	0.00	0.50	0.59	0.00	0.50	0.51	173.14	0.54
V_{max}/A_{max}	−0.16	0.00	0.00	−0.19	0.00	0.00	−0.19	0.00	0.00	−0.44	177.06	0.02
ACC RMS	0.89	0.08	0.84	0.89	0.11	0.82	0.91	0.12	0.82	0.77	6987.18	0.86
Vel RMS	0.82	0.00	0.72	0.82	0.00	0.71	0.84	0.00	0.71	0.70	169.42	0.72
Dis RMS	0.47	0.00	0.40	0.48	0.00	0.40	0.49	0.00	0.40	0.43	360.47	0.46
Arias Int.	0.47	0.01	0.87	0.48	0.01	0.86	0.49	0.01	0.85	0.41	636.00	0.89
I_c	0.62	0.03	0.87	0.63	0.04	0.85	0.64	0.05	0.85	0.54	3091.43	0.89
SED	0.42	0.00	0.73	0.43	0.00	0.71	0.44	0.00	0.71	0.36	45.37	0.72
CAV	0.89	0.00	0.76	0.89	0.00	0.74	0.91	0.00	0.74	0.76	3.62	0.77
ASI	0.91	0.02	0.85	0.91	0.03	0.84	0.93	0.03	0.84	0.81	2049.98	0.94
VSI	0.93	0.00	0.92	0.94	0.00	0.90	0.96	0.00	0.91	0.76	15.72	0.85
Housner Int.	0.91	0.00	0.90	0.92	0.00	0.88	0.94	0.00	0.88	0.75	18.06	0.83
SMA	0.92	0.02	0.86	0.93	0.03	0.85	0.95	0.03	0.85	0.81	2280.51	0.92
SMV	0.87	0.00	0.81	0.87	0.00	0.80	0.90	0.00	0.80	0.74	62.63	0.80
EDA	0.92	0.02	0.87	0.93	0.02	0.86	0.95	0.03	0.86	0.81	1883.16	0.92
A95	0.90	0.02	0.87	0.90	0.02	0.86	0.93	0.02	0.86	0.79	1786.21	0.92
T_p	0.39	0.01	0.07	0.43	0.01	0.08	0.44	0.01	0.08	0.18	555.55	0.02
T_m	−0.24	0.00	0.00	−0.25	0.00	0.00	−0.24	0.00	0.00	−0.80	310.30	0.08
I_f	0.91	0.00	0.83	0.91	0.00	0.81	0.93	0.00	0.81	0.77	26.28	0.82
I_{cm}	−0.33	0.00	0.03	−0.34	0.00	0.03	−0.35	0.00	0.03	−0.28	409.89	0.03
M	5.14	0.00	0.33	5.16	0.00	0.32	5.27	0.00	0.32	4.52	0.11	0.35
R	−0.47	0.01	0.14	−0.47	0.01	0.13	−0.49	0.01	0.13	−0.38	1066.55	0.12
t_{smd}	−0.49	0.01	0.09	−0.50	0.02	0.09	−0.52	0.02	0.09	−0.45	1403.65	0.10
V_{s30}	0.17	0.00	0.01	0.23	0.00	0.01	0.24	0.00	0.01	0.00	459.46	0.00
$S_a(T_1)$	0.88	0.01	0.98	0.89	0.02	0.97	0.91	0.02	0.97	0.70	1131.01	0.84
$S_a(1.5T_1)$	0.87	0.01	0.88	0.87	0.02	0.86	0.89	0.02	0.86	0.70	1477.65	0.78
$S_a(2T_1)$	0.77	0.02	0.77	0.77	0.02	0.75	0.79	0.02	0.75	0.63	1679.34	0.70
$S_a(T_2)$	0.88	0.01	0.81	0.88	0.01	0.80	0.90	0.01	0.80	0.80	952.16	0.93
$S_a(T_3)$	0.82	0.01	0.76	0.83	0.01	0.75	0.85	0.01	0.74	0.75	933.79	0.87
$S_v(T_1)$	0.88	0.00	0.98	0.89	0.00	0.97	0.91	0.00	0.97	0.70	38.06	0.84
$S_d(T_1)$	0.88	0.00	0.98	0.89	0.00	0.97	0.91	0.00	0.97	0.70	154.51	0.84
Cor. Int.	0.94	0.01	0.95	0.95	0.02	0.94	0.97	0.02	0.94	0.77	1175.03	0.88
Mod. Cor. Int.	0.92	0.01	0.92	0.93	0.01	0.91	0.95	0.01	0.91	0.77	1051.21	0.88
Two period Int.	0.89	0.01	0.98	0.90	0.02	0.97	0.92	0.02	0.97	0.71	1131.93	0.86
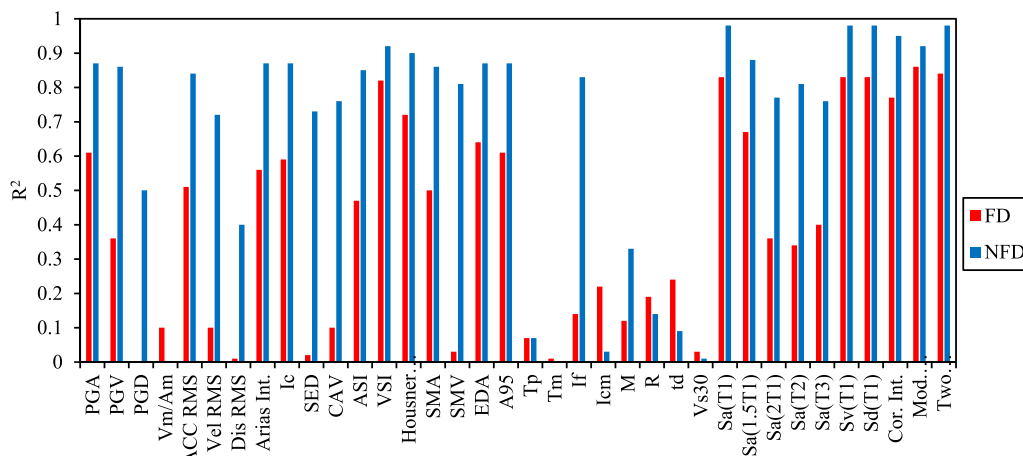
Fig. 9. The goodness of fitting R^2 value for various IMs versus MRDR.

6.3. Practicality

As discussed above, the practicality of the IMs in this study is examined by the slope, b, of the PSDM. A more practical IM yields a larger b. However, this method is not suitable for selecting the best IMs on its own, and it should be used with other criteria. The
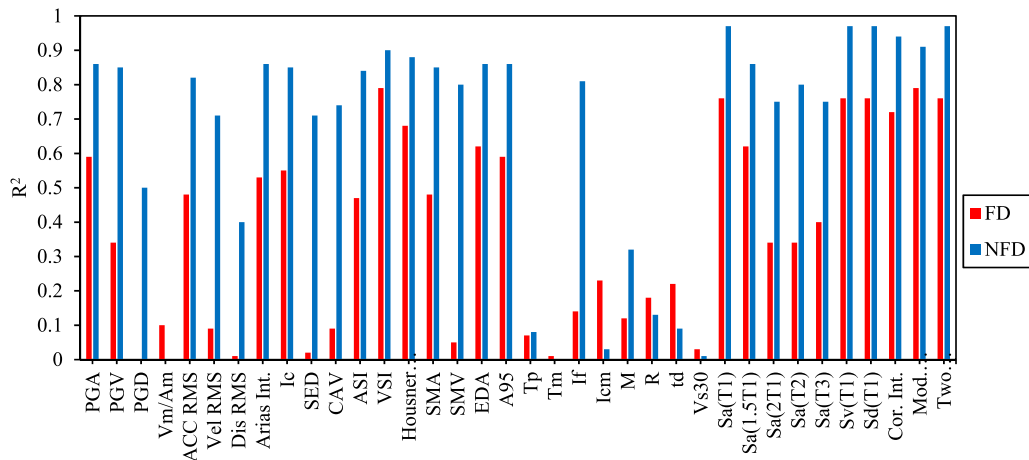
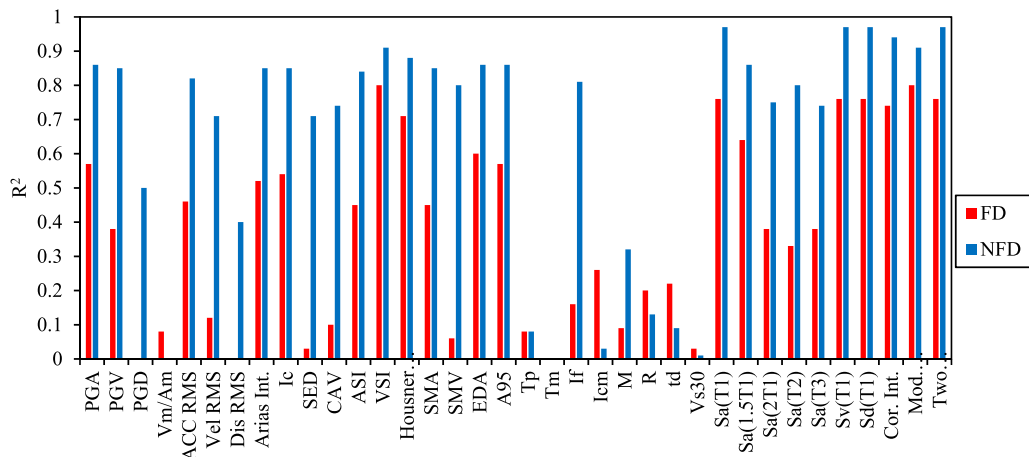**Fig. 10.** The goodness of fitting R^2 value for various IMs versus IDRCF.

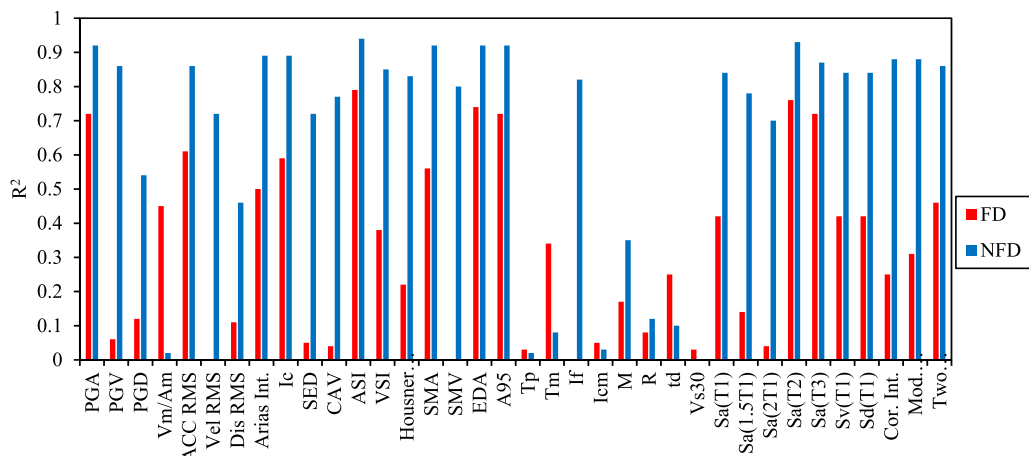**Fig. 11.** The goodness of fitting R^2 value for various IMs versus IDRFF.

Fig. 12. The goodness of fitting R^2 value for various IMs versus MCA.
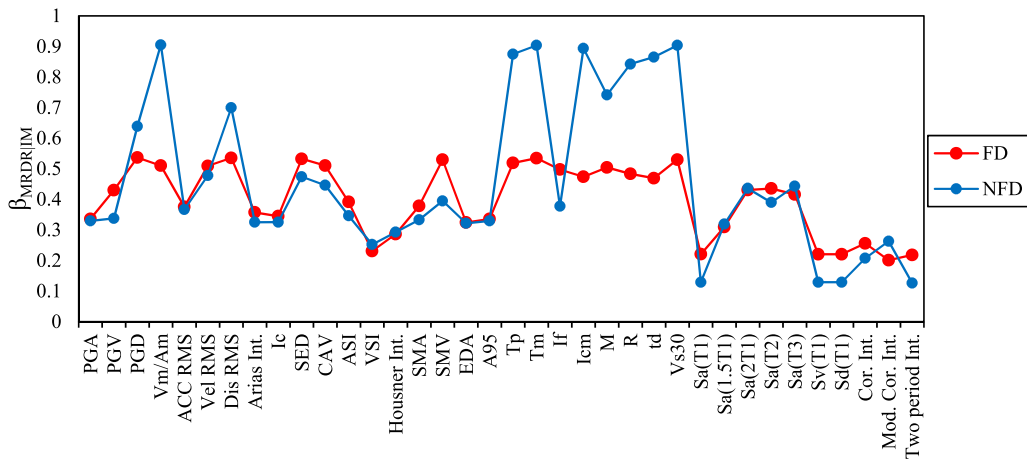
Fig. 13. Regression parameter β$_{EDP|IM}$ between IMs against MRDR as EDP subjected to near-field ground motions.
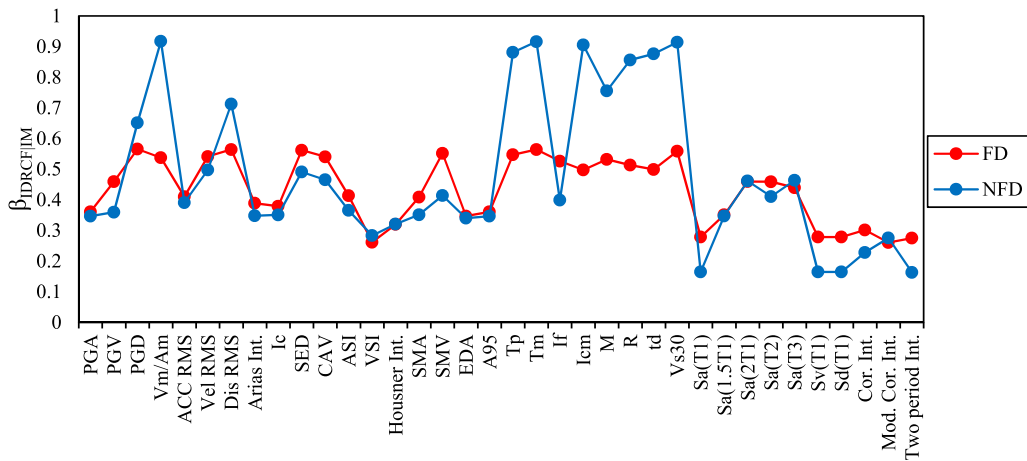

Fig. 14. Regression parameter β$_{EDP|IM}$ between IMs against IDRCF as EDP subjected to near field ground motions.
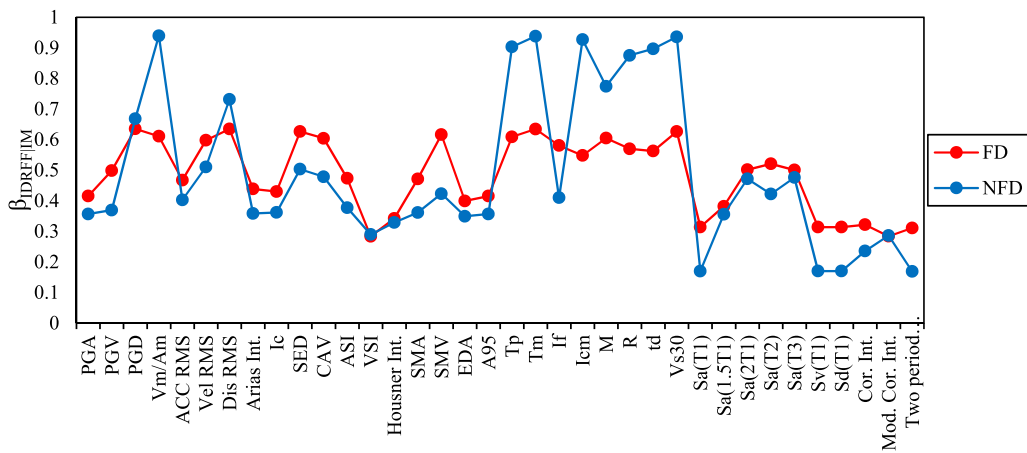

Fig. 15. Regression parameter β$_{EDP|IM}$ between IMs against IDRFF as EDP subjected to near-field ground motions.

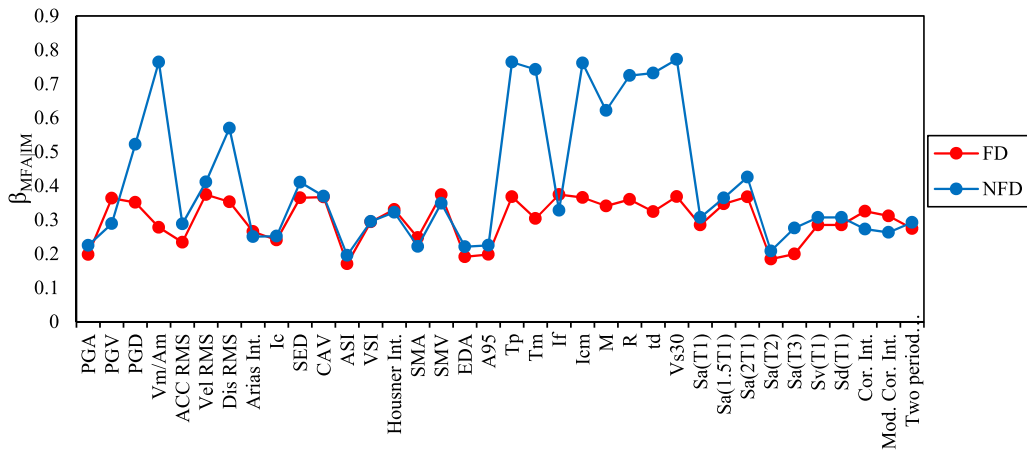**Fig. 16.** Regression parameter $\beta_{EDP|IM}$ between IMs against MCA as EDP subjected to near-field ground motions.

Fig. 17. Regression coefficient, b, corresponding to the MRDR, obtained from the cloud analysis subjected to near-field ground motion.

Fig. 18. Regression coefficient, b, corresponding to the IDRCF, obtained from the cloud analysis subjected to near-field ground motions.
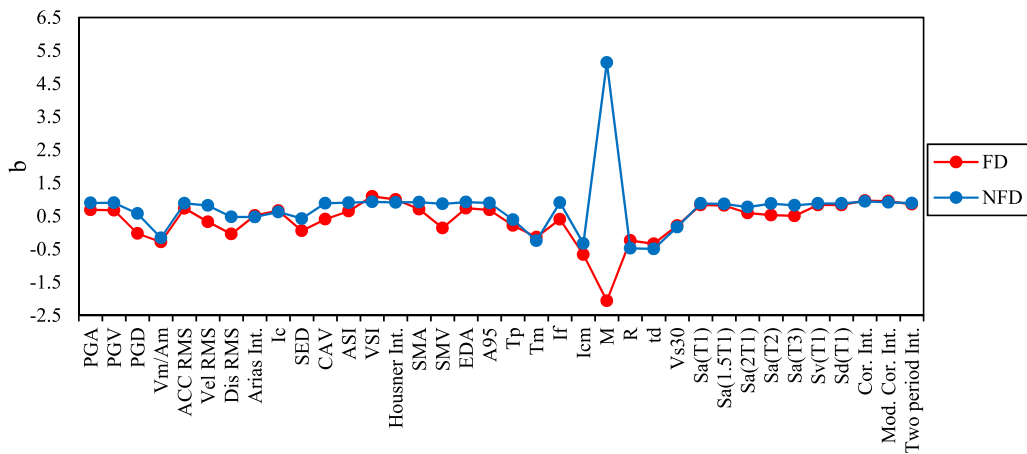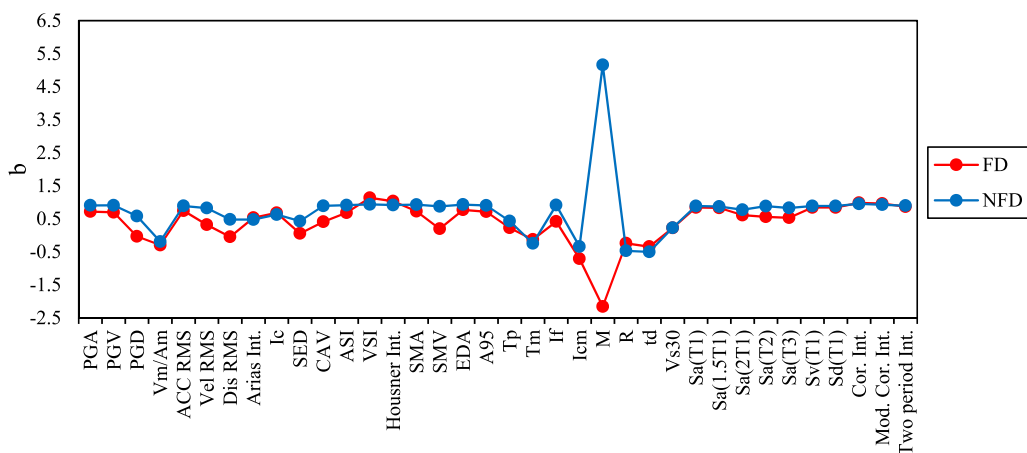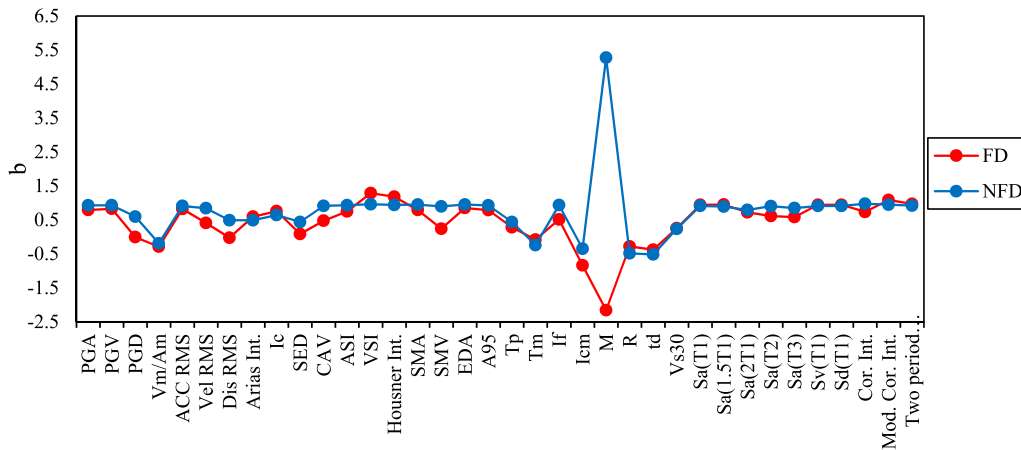
Fig. 19. Regression coefficient, b, corresponding to the IDRFF, obtained from the cloud analysis subjected to near-field ground motions.
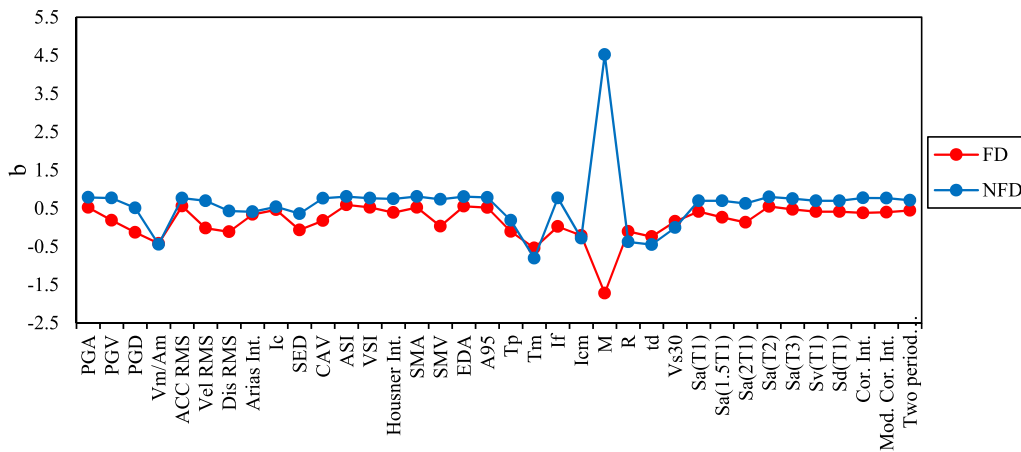

Fig. 20. Regression coefficient, b, corresponding to the MCA, obtained from the cloud analysis subjected to near-field ground motions.

practical comparison of the four selected EDPs against IMs is shown in Figs. 17–20. According to Table 4, although the practicability of the selected intensity measures in each IMs category under the action of FD ground motions is approximately equal to those under the action of NFD ground motions, coefficient b (slope of linear regression) in the majority of IMs under the action of NFD records are higher than FD records. However, IM = M has an entirely different regression coefficient b in each EDP. It is also important to note that if the value of b is near zero or negative, it means there is no relationship between structural response demand and IM. As a result, the b slope of IMs with negative values is ignored since it implies that the IM is unable to predict EDP accurately.

As illustrated in Fig. 17, under the action of FD records, VSI tends to be the most practical IM for the MRDR, followed by I_H and Cordova intensity. Their corresponding slope b values are 1.096, 1.003 and 0.967, respectively. In contrast, SED tends to be the least practical IM with the b value of 0.0571. The other two least practical IMs are SMV and T_p with b values of 0.14 and 0.21, respectively. Under the NFD ground motions, M, Cordova intensity and VSI are determined to be the most practicable IMs under NFD ground motions, with corresponding b values of 5.14, 0.94, and 0.93, respectively. On the other hand, V_{S30}, T_p and SED (with regression coefficient b values of 0.16, 0.39 and 0.42, respectively) are the least practical IM for MRDR under NFD ground motions.

Fig. 18 reveals that the order of the first three most and the least practical IMs under FD records are similar to MRDR. However, their corresponding b value for practical IMs are 1.13, 1.03 and 0.98, respectively and for impractical IMs are 0.05, 0.19 and 0.22, respectively. Similarly, under NFD ground motions, the most practical IMs for IDRCF is M, followed by S_a^c and VSI. Their b values are 5.15, 0.95 and 0.93, respectively. The least IMs under these ground motions are V_{S30} (b = 0.22), T_p (b = 0.43) and SED (b = 0.42).

As shown in Fig. 19, VSI appears to be the most practical IM for IDRFF under FD ground motions since it has the maximum slope b of 0.86. The second and third most practical IMs belong to I_H and S_a^c* with the b slope of 1.18 and 1.08, respectively. In contrast, SED, SMV, and VS30 are the least practical IMs among other IMs with their corresponding b slope of 0.08, 0.23 and 0.25. Under the action of NFD records, IM = M is found to be the most practical IM with b value of 5.27. The two next practical IMs are S_a^c and VSI with b values of 0.95 and 0.97, respectively. However, the least IMs are as same as IDRCF.

Taking into account MCA as EDP and FD records as input ground motions, it shows that acceleration-related IMs, including ASI with

the b value of 0.58 and A_{rms} and EDA with the b value of 0.55 for both, are found to be the most practical IMs. I_f, SMV and $S_a(2T_1, \zeta)$ with b values of 0.02, 0.03 and 0.13, respectively, are the least practical IMs. IMs such as M, ASI and SMA with b value of 4.52 for M and 0.80 for the two next IMs, are the most practical IMs under NFD records. On the other hand, with b value of 0.18, T_p is selected as the least practical IM. The next least practical IMs are SED and Arias intensity with b values of 0.35 and 0.4, respectively.

6.4. Sufficiency

The term sufficiency refers to the correlation that exists between the ground motion information parameter (IM_i) and the ground motion parameter (magnitude M or source-to-site distance R). A sufficient ground motion parameter should be statistically independent of the ground motion information parameter. The p-value of regression analysis would be smaller than the given significance threshold if the demand residuals and seismic information parameters are not statistically independent of each other, demonstrating that IM_i is insufficient. The limit for an insufficient IM_i is set at a p-value of 0.05. The sufficiency of IM would be stronger if the p-value value is higher. *The lower slope of the regression line indicates a sufficient IM independent of ground motion properties, indicating that the demand models are sufficient to ignore the conditional probability.* As an example, for both FD and NFD records, the residuals of the MRDR versus VSI and Two-period intensity are displayed in terms of M and R in Fig. 21. Under the action of FD records, Two-period intensity is sufficient than VSI with respect to the M. However, the opposite trend is seen with respect to the R.

In order to find sufficient IMs, the linear regression slope of the IM-EDP residuals under FD and NFD earthquake ground motions are tabulated in Table 6 and Table 7. In the majority of IMs for both NFD and FD near-fault ground motions, the linear regression slope of the IM-EDP residuals is less when R is used rather than M, according to Tables 6 and 7. Thus, it validates the commonly accepted assumption that R is generally preferred over M. In this section, sufficient IMs are selected based on the linear regression slope of Res-R for engineering demand parameters. It should be noted that most of the IM-EDP pairs have lower Res-R slope values under NFD records compared to FD records and belong to earthquake-based IMs.

Considering MRDR as EDP, the first three most sufficient IMs under FD records belong to VSI, I_c and R with the Res-R value of 0.003 for three IMs. Under NFD records, IM= SMA, PGA and A95 tend to be the sufficient IM with corresponding Res-R values of 0.0007 and 0.0008, respectively.

The sufficient IMs against IDRCF as EDP under FD records' action is precisely the same as IM-MRDR pairs. Similarly, the order of sufficient IMs under the action of NFD records is the same as the IM-MRDR pair. However, their corresponding Res-R values are 0.0001, 0.0005 and 0.0006.

The computed Res-R slope values for IDRFF under FD ground motions reveal that R, VSI and Arias intensity have the lowest value of 0.002, 0.004 and 0.006, respectively. The sufficient IMs under NFD ground motions are SMA, PGA and A95 with Res-R values of 0.006
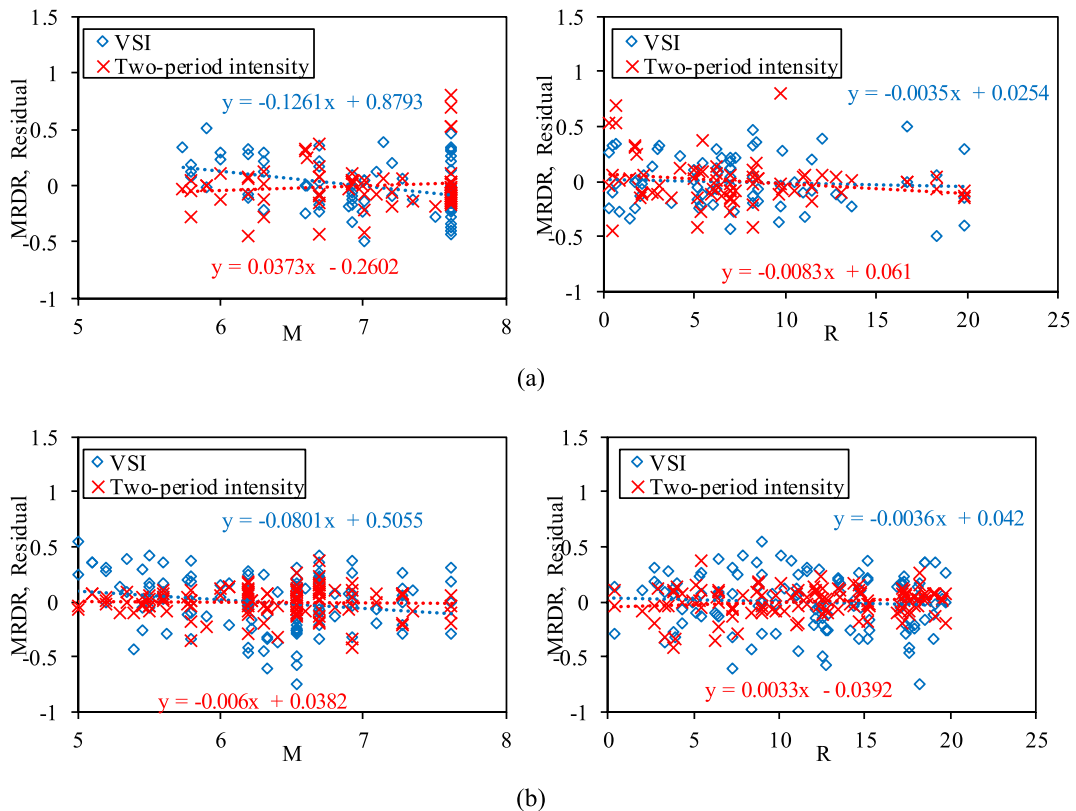

Fig. 21. Investigating the sufficiency of VSI and Two-period intensity with respect to M and R for predicting MRDR (a) FD records (b) NFD records.

Table 6

linear regression slope of the IM-EDP residuals under FD ground motions.

IM	Engineering Demand Parameters							
	MRDR		IDRCF		IDRFF		MCA	
	Res- M	Res- R	Res- M	Res- R	Res- M	Res- R	Res- M	Res- R
PGA	0.022	−0.006	0.020	−0.006	0.054	−0.009	−0.009	0.002
PGV	−0.430	−0.015	−0.449	−0.015	−0.473	−0.016	−0.295	−0.018
PGD	−0.283	−0.044	−0.290	−0.045	−0.319	−0.051	−0.115	−0.031
V_{max}/A_{max}	−0.127	−0.040	−0.132	−0.041	−0.138	−0.048	0.013	−0.021
ACC RMS	0.003	−0.011	−0.008	−0.011	0.024	−0.014	−0.023	−0.001
Vel RMS	−0.431	−0.034	−0.444	−0.035	−0.478	−0.039	−0.255	−0.027
Dis RMS	−0.259	−0.044	−0.267	−0.046	−0.296	−0.052	−0.117	−0.029
Arias Int.	−0.223	−0.004	−0.236	−0.004	−0.227	−0.006	−0.204	0.000
I_c	−0.115	−0.004	−0.126	−0.004	−0.105	−0.006	−0.125	0.001
SED	−0.392	−0.041	−0.406	−0.042	−0.446	−0.047	−0.169	−0.029
CAV	−0.440	−0.034	−0.457	−0.035	−0.478	−0.040	−0.318	−0.022
ASI	−0.021	−0.017	−0.022	−0.016	0.006	−0.020	0.001	−0.002
VSI	−0.126	−0.003	−0.135	−0.003	−0.111	−0.004	−0.173	−0.007
Housner Int.	−0.244	−0.009	−0.258	−0.009	−0.249	−0.010	−0.236	−0.013
SMA	−0.040	−0.013	−0.048	−0.013	−0.025	−0.017	−0.062	−0.003
SMV	−0.347	−0.039	−0.377	−0.039	−0.388	−0.044	−0.270	−0.025
EDA	0.023	−0.008	0.023	−0.007	0.058	−0.010	−0.010	0.001
A_{95}	0.025	−0.007	0.023	−0.006	0.057	−0.009	−0.007	0.002
T_p	−0.371	−0.038	−0.389	−0.039	−0.405	−0.044	−0.232	−0.029
T_m	−0.264	−0.042	−0.283	−0.043	−0.300	−0.050	−0.076	−0.019
I_f	−0.481	−0.030	−0.502	−0.031	−0.543	−0.034	−0.272	−0.025
I_{cm}	−0.221	−0.030	−0.230	−0.030	−0.213	−0.034	−0.233	−0.022
M	−0.009	−0.042	−0.010	−0.043	−0.011	−0.049	−0.009	−0.025
R	−0.335	−0.003	−0.352	−0.003	−0.357	−0.003	−0.272	−0.008
t_{smd}	0.019	−0.030	0.011	−0.031	0.044	−0.036	−0.026	−0.017
V_{s30}	−0.304	−0.037	−0.320	−0.038	−0.320	−0.044	−0.257	−0.022
$S_a(T_1)$	0.027	−0.009	0.013	−0.010	0.053	−0.013	−0.094	−0.009
$S_a(1.5T_1)$	−0.226	−0.010	−0.241	−0.010	−0.230	−0.012	−0.235	−0.015
$S_a(2T_1)$	−0.349	−0.028	−0.366	−0.028	−0.374	−0.032	−0.270	−0.023
$S_a(T_2)$	−0.082	−0.020	−0.085	−0.019	−0.063	−0.023	−0.025	−0.001
$S_a(T_3)$	−0.053	−0.022	−0.056	−0.022	−0.031	−0.027	−0.021	−0.007
$S_v(T_1)$	0.026	−0.009	0.012	−0.010	0.052	−0.013	−0.095	−0.009
$S_d(T_1)$	0.026	−0.009	0.012	−0.010	0.052	−0.013	−0.095	−0.009
Cor. Int.	−0.147	−0.011	−0.160	−0.011	−0.203	−0.026	−0.197	−0.013
Mod. Cor. Int.	−0.070	−0.005	−0.083	−0.005	−0.053	−0.007	−0.161	−0.010
Two period Int.	0.037	−0.008	0.025	−0.009	0.065	−0.011	−0.081	−0.008

and 0.001 for the two latter IMs, respectively.

Considering MCA results obtained under FD records, Arias intensity is the sufficient IMs with the Res-R value of 0.0003 followed by EDA (Res-R value = 0.0005) and A_{rms} (Res-R value = 0.001). On the other hand, under NFD records, PGV, VSI and I_H are found to be sufficient IMs. Their residual response slope values are 0.0001, 0.0004 and 0.0005, respectively.

6.5. Proficiency

By combining practicality and efficiency, the composite measure ζ can be used to estimate the proficiency of IMs. A more proficient IM has a lower ζ. Fig. 22 displays the normalized dispersion or proficiency coefficient ζ for all considered IM-EDP pairs under both FD and NFD records. It is obvious that IM-EDP pairs are more proficient under NFD ground motions compared to those under FD ground motions. The value of ζ for the M is low when investigating the IMs proficiency, but this should be ignored since, as previously mentioned, proficiency is a composite measure of practicability and efficiency. Earthquake magnitude (M), on the other hand, cannot be used as a criterion because of its high $β_{EDP|IM}$ value.

The first three most proficient IMs under FD records for all EDPs except MCA are VSI, I_H, and $S_a(T_1,ζ)$. For MCA, the most proficient IMs are ASI, $S_a(T_2,ζ)$, and EDA. Under NFD records, however, each EDP has different proficient IMs. As coupled with MRDR, $S_a(T_1,ζ)$, VSI and I_H are the most proficient IMs. Considering IDRCF and IDRFF as EDP reveals that the most proficient IMs belong to S_a^{tp}, $S_a(T_1,ζ)$ and $S_v(T_1,ζ)$, respectively. For MCA under the NFD ground motions, the most proficient IMs are found similar to MCA under FD ground motions.

Based on the previous tests, the three most correlated, efficient, sufficient, practical, and proficient IMs for four selected EDPs were calculated under the action of FD and NFD ground motions. It can be shown that for deformation-based EDPs such as MRDR, IDRCF, and IDRFF, IM= VSI, S_a^{tp}, and $S_a^{c}*$ are appropriate IMs for the two types of near-field records since they are among the best five optimal IMs for each mentioned criteria. $S_a(T_1,ζ)$ can also be good IM to predict EDPs. Furthermore, changing EDP from deformation-based engineering demand parameters to MCA demonstrates that ASI and EDA are the best options to predict MCA.

Table 7

linear regression slope of the IM-EDP residuals under FD ground motions.

IM	Engineering Demand Parameters							
	MRDR		IDRCF		IDRFF		MCA	
	Res- M	Res- R	Res- M	Res- R	Res- M	Res- R	Res- M	Res- R
PGA	−0.020	−0.001	−0.023	−0.001	−0.024	−0.001	−0.018	0.006
PGV	−0.072	−0.006	−0.073	−0.006	−0.075	−0.007	−0.042	0.000
PGD	0.093	−0.032	0.090	−0.032	0.093	−0.034	0.073	−0.021
V_{max}/A_{max}	0.840	−0.064	0.845	−0.064	0.865	−0.067	0.751	−0.047
ACC RMS	−0.043	−0.008	−0.043	−0.008	−0.044	−0.009	−0.029	−0.001
Vel RMS	−0.047	−0.021	−0.047	−0.021	−0.048	−0.023	−0.019	−0.013
Dis RMS	0.145	−0.043	0.144	−0.044	0.149	−0.045	0.106	−0.030
Arias Int.	−0.137	−0.009	−0.139	−0.009	−0.142	−0.010	−0.109	−0.001
Ic	−0.113	−0.008	−0.114	−0.008	−0.116	−0.009	−0.088	−0.001
SED	−0.108	−0.023	−0.109	−0.024	−0.112	−0.025	−0.068	−0.015
CAV	−0.144	−0.023	−0.145	−0.023	−0.148	−0.024	−0.111	−0.013
ASI	−0.021	−0.006	−0.023	−0.006	−0.023	−0.007	−0.033	0.003
VSI	−0.080	−0.004	−0.081	−0.004	−0.083	−0.004	−0.020	0.000
Housner Int.	−0.088	−0.005	−0.088	−0.005	−0.091	−0.006	−0.025	−0.001
SMA	−0.014	0.000	−0.017	0.000	−0.018	−0.001	−0.015	0.007
SMV	−0.096	−0.008	−0.097	−0.008	−0.101	−0.009	−0.056	−0.002
EDA	−0.036	−0.002	−0.039	−0.002	−0.040	−0.003	−0.030	0.005
A_{95}	−0.016	−0.001	−0.020	−0.001	−0.020	−0.001	−0.015	0.006
T_p	0.766	−0.069	0.763	−0.070	0.781	−0.072	0.697	−0.052
T_m	0.828	−0.064	0.831	−0.064	0.850	−0.066	0.714	−0.045
I_f	−0.117	−0.012	−0.118	−0.012	−0.121	−0.013	−0.078	−0.005
I_{cm}	0.863	−0.059	0.867	−0.059	0.887	−0.061	0.754	−0.045
M	0.005	−0.048	0.005	−0.048	0.006	−0.050	0.000	−0.035
R	0.728	−0.009	0.732	−0.010	0.747	−0.010	0.644	−0.005
t_{smd}	0.916	−0.051	0.921	−0.051	0.942	−0.053	0.804	−0.037
V_{s30}	0.817	−0.064	0.815	−0.064	0.833	−0.066	0.728	−0.050
$S_a(T_1)$	0.003	0.003	0.000	0.003	0.000	0.003	0.073	0.004
$S_a(1.5T_1)$	−0.022	−0.007	−0.021	−0.007	−0.023	−0.008	0.042	−0.003
$S_a(2T_1)$	−0.011	−0.011	−0.008	−0.012	−0.009	−0.013	0.044	−0.007
$S_a(T_2)$	0.012	−0.006	0.011	−0.006	0.012	−0.007	−0.018	0.004
$S_a(T_3)$	0.055	−0.011	0.055	−0.011	0.057	−0.012	0.018	−0.001
$S_v(T_1)$	0.003	0.003	0.000	0.003	0.000	0.003	0.073	0.004
$S_d(T_1)$	0.003	0.003	0.000	0.003	0.000	0.003	0.073	0.004
Cor. Int.	−0.030	−0.005	−0.035	−0.005	−0.036	−0.006	0.022	−0.001
Mod. Cor. Int.	−0.009	−0.010	−0.015	−0.009	−0.014	−0.011	0.024	−0.004
Two period Int.	−0.006	0.003	−0.009	0.004	−0.010	0.003	0.060	0.004

7. Vulnerability (fragility) function

As described in Section 2, fragility analysis is one of the most effective methods for evaluating structures' seismic vulnerability, as it provides the probability of collapse or other limit states of interest as a function of some ground motion intensity measure (IM). The fragility analysis includes the selection of uncertainty, intensity measure, damage measure for seismic demands, damage states, and the generation of the fragility curve. The fragility function determines the probability of reaching or exceeding a specific damage state for a given set of input intensity variables.

Using nonlinear time history responses of MBS under near-field ground motions, this study uses the Probabilistic Seismic Demand Model (PSDM) to construct analytical fragility functions. To link engineering demand parameters (EDPs) to ground motion intensity measures (IMs), the PSDM is created utilizing the "cloud" technique. Due to the fact that VSI, S_a^{tp}, $S_a^{c}*$ and $S_a(T_1,\zeta)$ were shown to be strong predictors of MBS's structural responses under both FD and NFD records, the conditional probability of failure is determined utilizing these four parameters as the IM.

EDP selection is critical since it determines structures' elastic and inelastic states [68,69]. The maximum inter-story drift ratio is the most significant EDP in the evaluation of the fragility of frame structures, and it is used to evaluate the local and global story collapse. In the present study, among the four EDPs mentioned earlier, IDRFF is chosen for fragility analysis because, in most cases, the results obtained for this EDP were more critical than those obtained for IDRCFF. The exceedance probability of two damage levels is analyzed. The damage state considered for IDRFF is 0.02 for LS and 0.04 for CP.

Fig. 23 shows the fragility curves generated from optimum IMs. The probability of exceeding 0.02 for FD records is higher than for NFD records; however, raising the IMs values except for $S_a^{c}*$ brings the likelihood of IDRFF exceeding 0.02 closer. Furthermore, the probability of exceeding 0.04 for the MBS under FD ground motions is higher than that of NFD records among all types of IMs and damage states. At a constant optimal IMs, the probability of exceedance of the LS damage state is higher than that of the CP damage state. It is also worth noting that the fragility curve's horizontal elongation indicates lower hand estimations, whereas the vertical elongation indicates higher hand estimates. Furthermore, it is discovered that under the action of NFD records, the probability of exceeding the considered damage state is more sensitive to IMs than under the action of FD records.
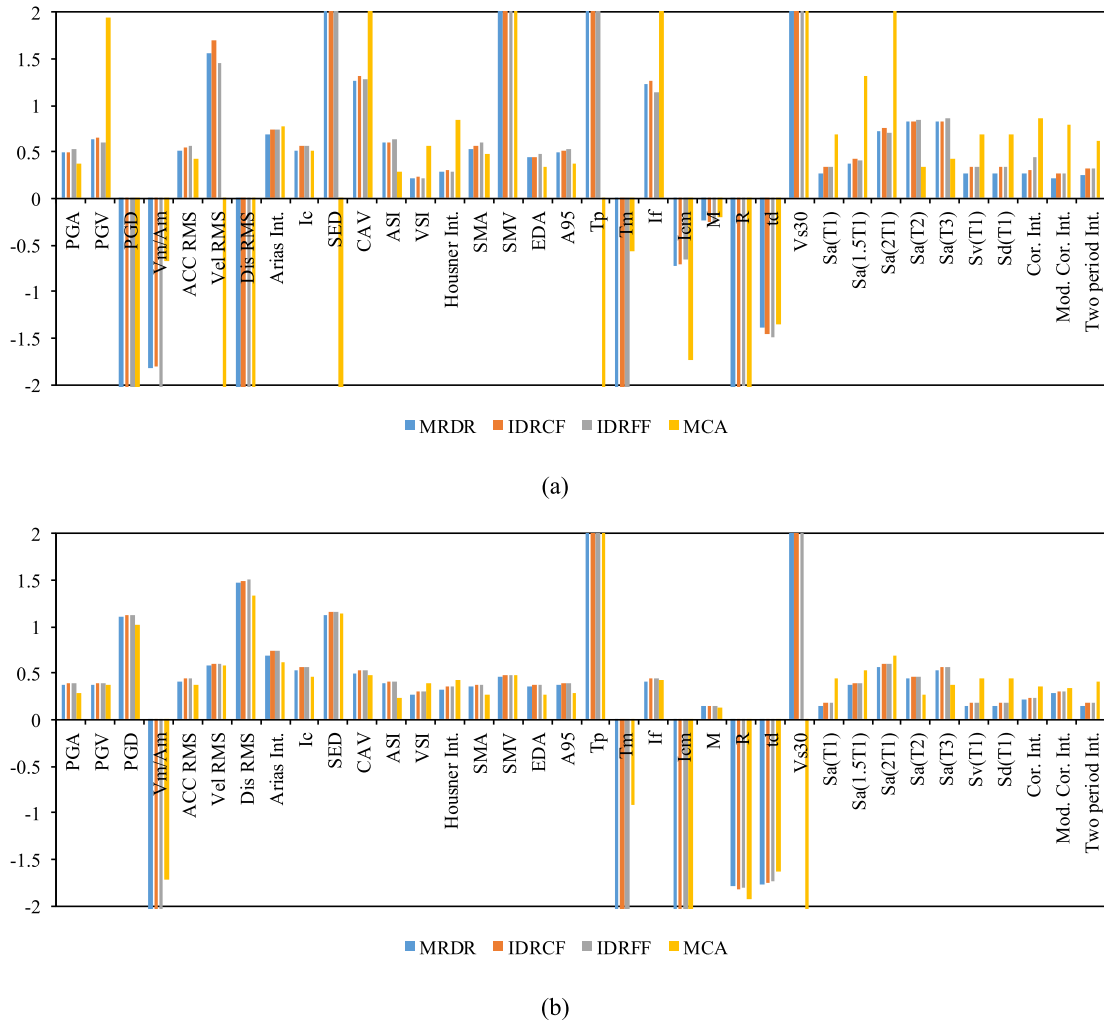
(a)

(b)

Fig. 22. The proficiency values fore considered IM-EDP pairs (a) FD records (b) NFD records.

8. Structural demand hazard curves (SDHC)

The seismic demand hazard is a suitable metric for assessing the seismic performance of a structure due to ground shaking since it takes into account both the probability of different levels of ground motion shaking at a location and the link between ground motion shaking and seismic response, including its uncertainty. A PSDM can be integrated with Probabilistic Seismic Hazard Analysis (PSHA) to provide a comprehensive Probabilistic Seismic Demand Analysis (PSDA) and structural "demand hazard curves" [70,71] represented as:

$$\Lambda(EDP \geq \alpha) = \int_{IM} P[EDP \geq \alpha | IM = \beta] \left| d\lambda(\beta) \right| \tag{9}$$

where $\Lambda(EDP \geq \alpha)$ is the mean annual frequency exceeding a capacity level (α) and $\lambda(\beta)$ determines the exceeding annual likelihood of earthquake IM for a particular location. The following exponential form [46] can be used to estimate the site hazard curve:

$$P[IM \geq \beta] = k_0(\beta)^{-k} \tag{10}$$

Considering the hazard curve is linear on a log-log plot, Eq. (9) can be integrated using Eq. (11) and an exponential fit to the PSDM to obtain:

$$P[EDP \geq \alpha] = k_0 \left[\left(\frac{\alpha}{a} \right)^{1/b} \right]^{-k} . e^{\left[\frac{K^2 \sigma_{EDP|IM}^2}{2b^2} \right]} \tag{11}$$
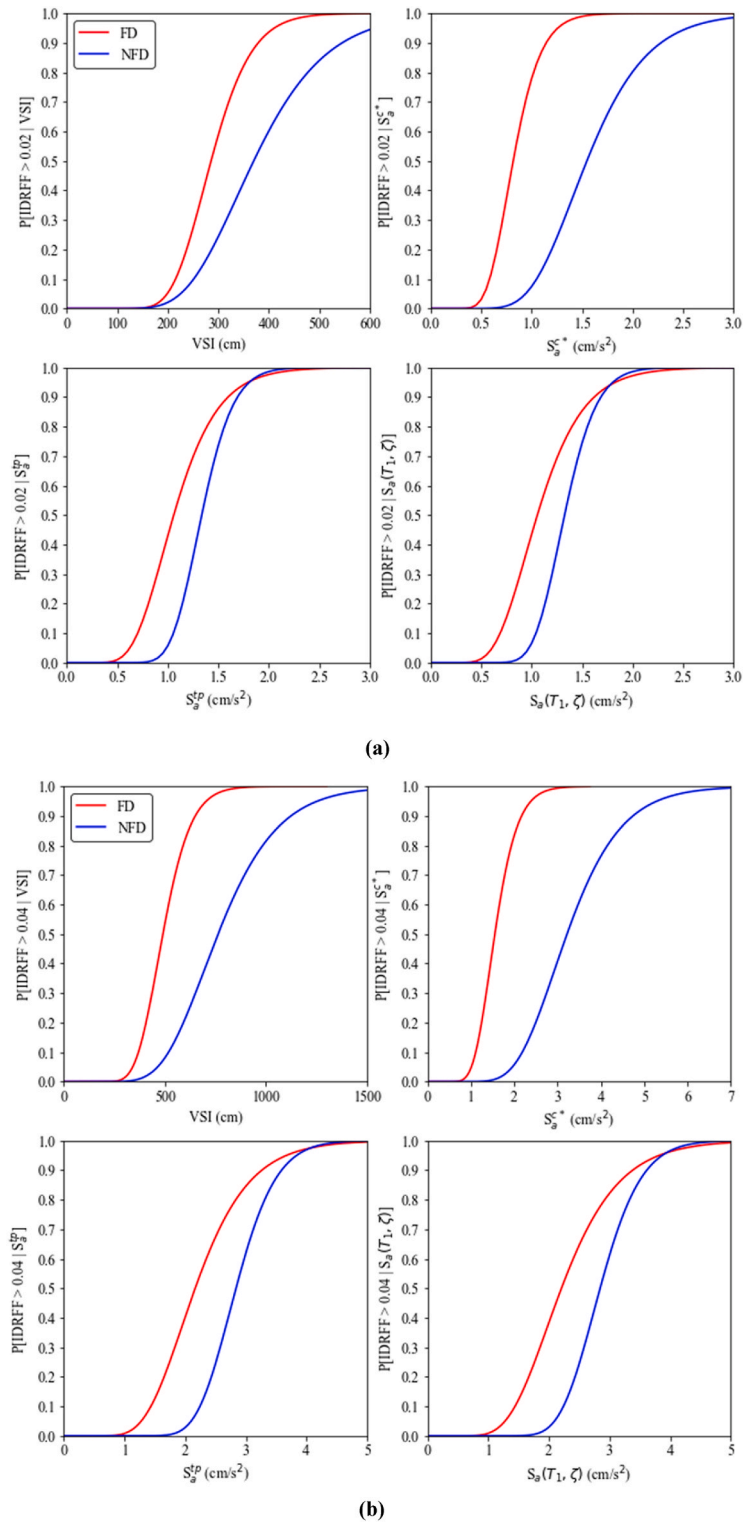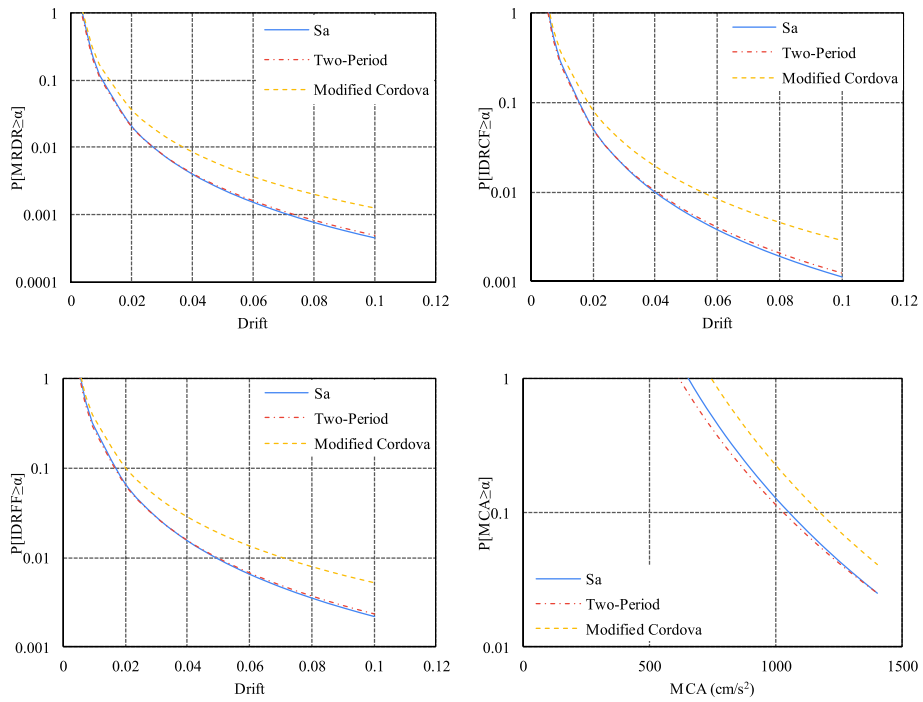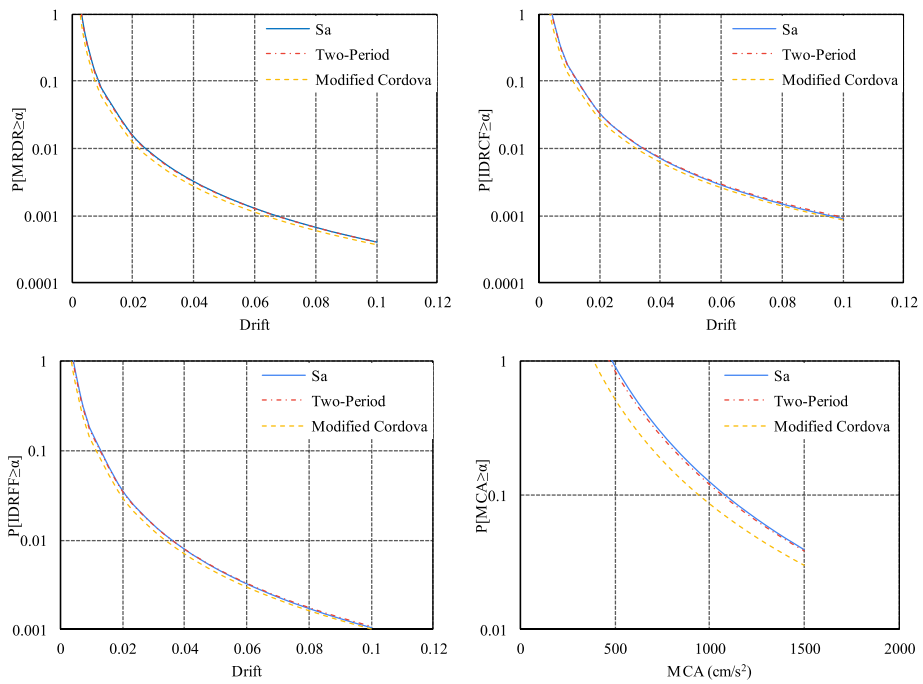
Fig. 23. Fragility curves of maximum inter-story drift ratios (IDRFF) for (a) LS performance state of optimal intensity measures (b) CP performance state of optimal intensity measures.

(a)

(b)

Fig. 24. Structural response hazard curves computed using optimal IMs; (a) FD records (b) NFD records.
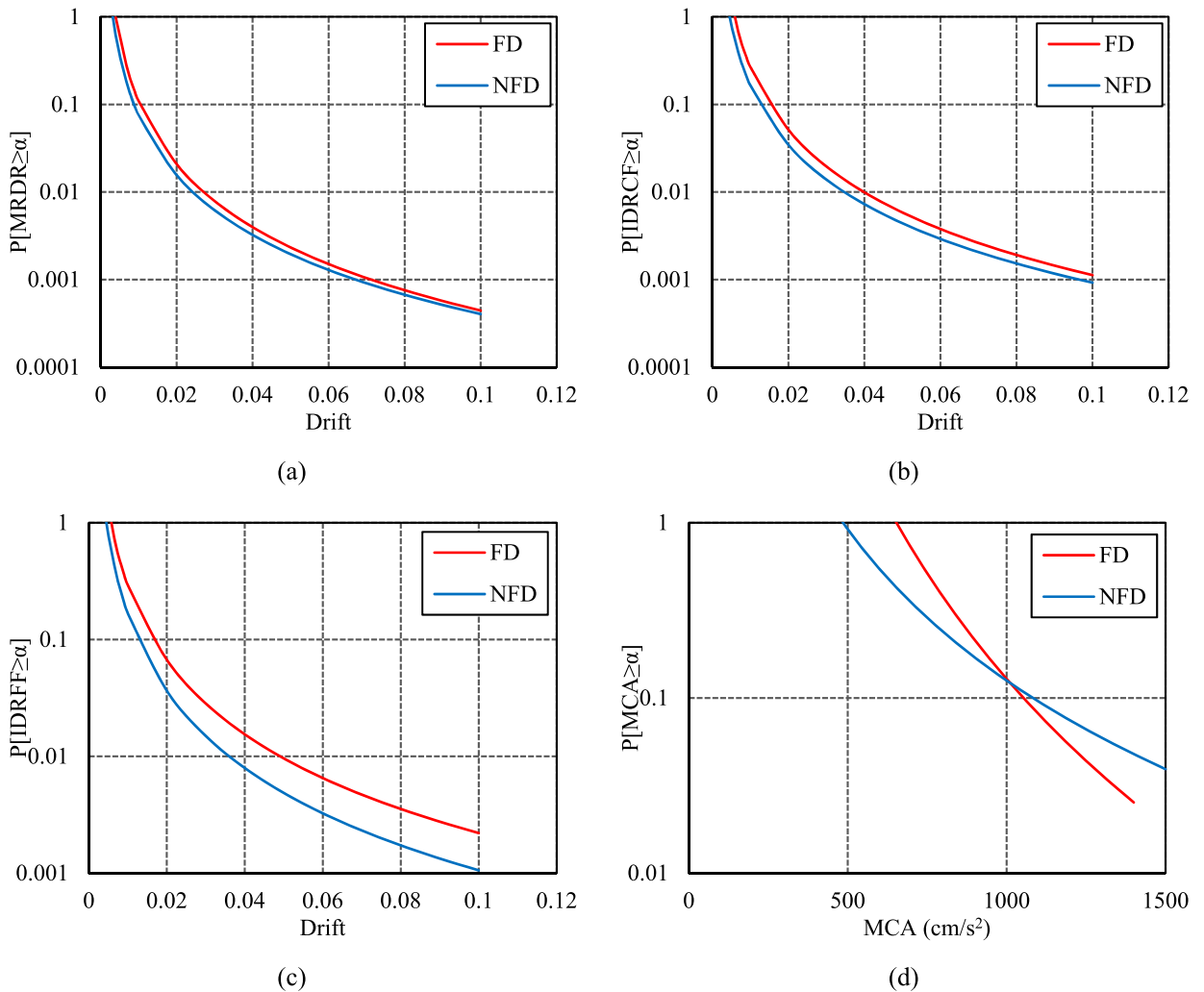
Fig. 25. Structural response hazard curves computed using Sa (T₁,ζ).

In Eq. (4), the values for the parameters a and b were determined. The PSDMs are integrated with individual site PSHA to provide structural demand hazard curves. To depict SDHC, the optimal IMs of S_a^{tp}, $S_a^{c}*$, and $S_a(T_1,\zeta)$ were chosen, as shown in Fig. 24. However, the structural response hazard curve using optimal IM=VSI has not been reported due to the low probability of occurrence of EDPs in the MBS, mainly as a result of the low coefficient of a (as illustrated in Table 4 and Table 5). From this figure, it can be seen that under the two sets of records, the SDHC of the steel MBS with IM = S_a^{tp} and $S_a(T_1,\zeta)$ are close. However the SDHCs using the IM of $S_a^{c}*$ under the FD records are higher than the other IMS. The opposite trend was seen for NFD records. As an example, The SDHCs obtained using the appropriate IM of $S_a(T_1,\zeta)$ are constructed and displayed in Fig. 25 using arbitrary values of k = 2 and k_0 = 0.06 [72]. Accordingly, it can be observed that in the deformation-based EDPs, demand hazard curves obtained for MBS under FD records are higher than in NFD records. The demand hazard curve of MRDR shows that the structure certainly experiences 0.4% total drift under two types of near-field ground motions. Fig. 25(b) depicts that the probability of 2% drift for MBS is 5% and 3.4% under the action of FD and NFD records, respectively. This probability for IDRFF under FD and NFD records is 6% and 3.6%, respectively. However, Fig. 25(d) shows that in the same value of MCA between 500 and 1000 cm/s² the probability of MCA for MBS under FD records is higher than in NFD records. In contrast, the opposite trend is observed from 1000 cm/s² onwards.

9. Comparison of the results for MBSs with other studies

In the literature, there has been no study examining the optimal IMs for mid-rise steel Modular Building Systems (MBS). The results of the present study are presented in Table 8 along with those of other studies conducted on various buildings to compare the optimal IMs determined by the present study for MBS and the applicability of the current conclusion to other more common types of structural systems. According to the table, different optimal IMs were obtained for different buildings. Therefore, the optimal IM obtained for the MBS may not be appropriate for another and cannot be extended to other more common structural systems.

Table 8

Optimal IMs for various types of buildings.

Building type	Optimal IMs	Ref.
Steel MRF	$S_a(T_1,\zeta)$	[45]
Steel diagrid systems	PGV and PGV/PGA	[22]
Reinforced concrete (RC) building with hysteretic dampers	Modified Housner Intensity and Modified ASI	[73]
plan-irregular RC buildings	$Sa_{avg,GM}$	[74]
Medium-rise three dimensional	Sa (T_1,ζ), VSI, PGV and Ia	[75]
Mid-rise steel MBS (this study)	VSI, S_a^{tp}, and S_a^c *	–

10. Concluding remarks

Creating appropriate potential seismic demand models (PSDMs) is a significant part of the probabilistic performance-based approach. This research aims to assess the seismic vulnerability of mid-rise steel Modular Building Systems (MBSs) subjected to near-field ground motions by finding suitable intensity measures for developing PSDMs for mid-rise MBSs. In the context of Cloud analysis, two sets of near-field ground motions were chosen: 72 pulse-like and 120 non-pulse-like ground motions. Using 2D nonlinear dynamic analyses and the finite-element OpenSees software, numerical simulation models of the MBS were evaluated. To capture and monitor the results of the MBS, four engineering demand parameters were chosen: MRDR, IDRCF, IDRFF, and MCA. A total of 36 IMs were examined to find the optimality criteria of correlation, efficiency, practicality, and proficiency. It was indicated that other earthquake features of near-filed ground motions have a more significant impact than pulse, and the pulse nature scatters the MBS's seismic response. It was also found that as T_p/T_1 increases, the seismic responses of the MBS decrease in the EDPs, namely, MRDR, IDRCF, and IDRFF. The results also showed that VSI, Two-period intensity, Modified Cordova intensity, and acceleration response spectra at the fundamental period are the optimal IMs for deformation-based EDPs in the seismic vulnerability of the MBS under both types of near-field earthquake records. Moreover, ASI and EDA are the best IMs for MCA. This observation demonstrates that PGA, the most prevalent measure, is not necessarily the optimal IM for seismic fragility analysis of mid-rise MBSs. At last, the MBS's seismic vulnerability was examined by combining the PSDM and a PSHA to produce seismic fragility curves under the action of FD and NFD records, and structural demand hazard curves were generated by combining the PSDM and a PSHA.

Authorship statement

All persons who meet authorship criteria are listed as authors, and all authors certify that they have participated sufficiently in the work to take public responsibility for the content, including participation in the concept, design, analysis, writing, or revision of the manuscript. Furthermore, each author certifies that this material or similar material has not been and will not be submitted to or published in any other publication before its appearance in *Journal of Building Engineering*.

Declaration of competing interest

The authors declare that they have no known competing financial interests or personal relationships that could have appeared to influence the work reported in this paper.

Data availability

No data was used for the research described in the article.

Acknowledgments

References

[1] P. Sharafi, M. Rashidi, M. Alembagheri, A. Bigdeli, System identification of a volumetric steel modular frame using experimental and numerical vibration analysis, J. Architect. Eng. 27 (4) (2021), 04021032.

[2] M. Rashidi, P. Sharafi, M. Alembagheri, A. Bigdeli, B. Samali, Operational modal analysis, testing and modelling of prefabricated steel modules with different lsf composite walls, Materials 13 (24) (2020) 1–18.

[3] M. Alembagheri, P. Sharafi, M. Rashidi, A. Bigdeli, M. Farajian, Natural dynamic characteristics of volumetric steel modules with gypsum sheathed LSF walls: experimental study, Structures 33 (2021) 272–282.

[4] Y.S. Chua, J.Y.R. Liew, S.D. Pang, Modelling of connections and lateral behavior of high-rise modular steel buildings, J. Constr. Steel Res. 166 (2020), 105901.

[5] R. Sanches, O. Mercan, B. Roberts, Experimental investigations of vertical post-tensioned connection for modular steel structures, Eng. Struct. 175 (August) (2018) 776–789.

[6] M. Alembagheri, P. Sharafi, R. Hajirezaei, Z. Tao, Anti-collapse resistance mechanisms in corner-supported modular steel buildings, J. Constr. Steel Res. 170 (2020).

[7] M. Alembagheri, P. Sharafi, R. Hajirezaei, B. Samali, Collapse capacity of modular steel buildings subject to module loss scenarios: the role of inter-module connections, Eng. Struct. 210 (2020), 110373.

[8] M. Farajian, P. Sharafi, A. Bigdeli, H. Eslamnia, P. Rahnamayiezekavat, Experimental study on the natural dynamic characteristics of steel-framed modular structures, Buildings 12 (5) (2022) 587.

[9] B. Xu, J. Xia, H. Chang, R. Ma, L. Zhang, A comprehensive experimental-numerical investigation on the bending response of laminated double channel beams in modular buildings, Eng. Struct. 200 (October) (2019).

[10] M. Alembagheri, P. Sharafi, Z. Tao, R. Hajirezaei, K. Kildashti, Robustness of multistory corner-supported modular steel frames against progressive collapse, Struct. Des. Tall Special Build. 30 (18) (2021) e1896.

[11] Z. Wang, K.D. Tsavdaridis, Optimality criteria-based minimum-weight design method for modular building systems subjected to generalised stiffness constraints: a comparative study, Eng. Struct. 251 (2022), 113472.

[12] D.-A. Corfar, K.D. Tsavdaridis, A comprehensive review and classification of inter-module connections for hot-rolled steel modular building systems, J. Build. Eng. 50 (2022), 104006.

[13] K.A. Porter, An overview of PEER's performance-based earthquake engineering methodology, in: Proceedings of Ninth International Conference on Applications of Statistics and Probability in Civil Engineering, 2003, pp. 1–8.

[14] P. Giovenale, C.A. Cornell, L. Esteva, Comparing the adequacy of alternative ground motion intensity measures for the estimation of structural responses, Earthq. Eng. Struct. Dynam. 33 (8) (2004) 951–979.

[15] J.E. Padgett, B.G. Nielson, R. DesRoches, Selection of optimal intensity measures in probabilistic seismic demand models of highway bridge portfolios, Earthq. Eng. Struct. Dynam. 37 (5) (2008) 711–725.

[16] G.W. Housner, Spectrum Intensities of Strong-Motion Earthquakes, 1952.

[17] Z.K. Huang, K. Pitilakis, S. Argyroudis, G. Tsinidis, D.M. Zhang, Selection of optimal intensity measures for fragility assessment of circular tunnels in soft soil deposits, Soil Dynam. Earthq. Eng. 145 (2021), 106724. September 2020.

[18] X. Wang, A. Ye, J.E. Padgett, Fractional order optimal intensity measures for probabilistic seismic demand modeling of extended pile-shaft-supported bridges in liquefiable and laterally spreading ground, Soil Dynam. Earthq. Eng. 120 (2019) 301–315. May 2017.

[19] V. V Bertero, S.A. Mahin, R.A. Herrera, Aseismic design implications of near-fault San Fernando earthquake records, Earthq. Eng. Struct. Dynam. 6 (1) (1978) 31–42.

[20] Y. Bozorgnia, S.A. Mahin, Ductility and strength demands of near-fault ground motions of the Northridge earthquake, in: Proceedings, 6th US National Conference on Earthquake Engineering, 1998.

[21] P.G. Somerville, N.F. Smith, R.W. Graves, N.A. Abrahamson, Accounting for Near-Fault Rupture Directivity Effects in the Development of Design Ground Motions, vol. 319, ASME-PUBLICATIONS-PVP, 1995, pp. 67–82.

[22] M. Heshmati, V. Jahangiri, Appropriate intensity measures for probabilistic seismic demand estimation of steel diagrid systems, Eng. Struct. 249 (2021), 113260.

[23] H. Haghgou, M. Alembagheri, A. Bigdeli, Determination of optimal intensity measure for probabilistic seismic demand analysis of intake towers, Structures 34 (2021) 1998–2013. January.

[24] B. Wei, Z. Hu, X. He, L. Jiang, Evaluation of optimal ground motion intensity measures and seismic fragility analysis of a multi-pylon cable-stayed bridge with super-high piers in Mountainous Areas, Soil Dynam. Earthq. Eng. 129 (2020), 105945.

[25] K. Mackie, B. Stojadinović, Probabilistic seismic demand model for California highway bridges, J. Bridge Eng. 6 (6) (2001) 468–481.

[26] N. Luco, C.A. Cornell, Structure-specific scalar intensity measures for near-source and ordinary earthquake ground motions, Earthq. Spectra 23 (2) (2007) 357–392.

[27] J. Donaire-Ávila, F. Mollaioli, A. Lucchini, A. Benavent-Climent, Intensity measures for the seismic response prediction of mid-rise buildings with hysteretic dampers, Eng. Struct. 102 (2015) 278–295.

[28] J.R. Pejovic, N.N. Serdar, R.R. Pejovic, Optimal intensity measures for probabilistic seismic demand models of RC high-rise buildings, Earthq. Struct. 13 (3) (2017) 221–230.

[29] L. Jiang, J. Zhong, M. He, W. Yuan, Optimal seismic intensity measure selection for isolated bridges under pulse-like ground motions, Adv. Civ. Eng. 2019 (2019).

[30] Y. Yazdani, M. Alembagheri, Seismic vulnerability of gravity dams in near-fault areas, Soil Dynam. Earthq. Eng. 102 (2017) 15–24. March.

[31] M.A. Hariri-Ardebili, V.E. Saouma, Probabilistic seismic demand model and optimal intensity measure for concrete dams, Struct. Saf. 59 (2016) 67–85.

[32] L. Tian, H. Pan, R. Ma, Probabilistic seismic demand model and fragility analysis of transmission tower subjected to near-field ground motions, J. Constr. Steel Res. 156 (2019) 266–275.

[33] A. Emamikoupaei, A. Bigdeli, K.D. Tsavdaridis, Nonlinear seismic response of mid-rise modular buildings subjected to near-field ground motions, J. Constr. Steel Res. 201 (2023), 107696.

[34] J.C. Anderson, V. V Bertero, Uncertainties in establishing design earthquakes, J. Struct. Eng. 113 (8) (1987) 1709–1724.

[35] B. Alavi, H. Krawinkler, Consideration of near-fault ground motion effects in seismic design, Proceedings of the 12th World Conference on Earthquake Engineering 8 (2000) 2000.

[36] J.D. Bray, A. Rodriguez-Marek, Characterization of forward-directivity ground motions in the near-fault region, Soil Dynam. Earthq. Eng. 24 (11) (2004) 815–828.

[37] P.G. Somerville, N.F. Smith, R.W. Graves, N.A. Abrahamson, Modification of empirical strong ground motion attenuation relations to include the amplitude and duration effects of rupture directivity, Seismol Res. Lett. 68 (1) (1997) 199–222.

[38] H. Benioff, Mechanism and strain characteristics of the White Wolf fault as indicated by the aftershock sequence, Bull., Calif. Div. Mines 171 (1955) 199–202.

[39] A. Alonso-Rodr\'\iguez, E. Miranda, Assessment of building behavior under near-fault pulse-like ground motions through simplified models, Soil Dynam. Earthq. Eng. 79 (2015) 47–58.

[40] G.P. Mavroeidis, A.S. Papageorgiou, A mathematical representation of near-fault ground motions, Bull. Seismol. Soc. Am. 93 (3) (2003) 1099–1131.

[41] J.W. Baker, Quantitative classification of near-fault ground motions using wavelet analysis, Bull. Seismol. Soc. Am. 97 (5) (2007) 1486–1501.

[42] P.E.E.R. Center, PEER Strong Motion Database, University of California, Berkeley Berkeley, CA, 2000.

[43] F. Jalayer, Direct Probabilistic Seismic Analysis: Implementing Non-linear Dynamic Assessments, Stanford University, 2003.

[44] C.A. Cornell, H. Krawinkler, Progress and Challenges in Seismic Performance Assessment, in: PEER Center News, Univ. California, Berkeley, 2000, 3.

[45] N. Shome, C.A. Cornell, P. Bazzurro, J.E. Carballo, Earthquakes, records, and nonlinear responses, Earthq. Spectra 14 (3) (1998) 469–500.

[46] C.A. Cornell, F. Jalayer, R.O. Hamburger, D.A. Foutch, Probabilistic basis for 2000 SAC federal emergency management agency steel moment frame guidelines, J. Struct. Eng. 128 (4) (2002) 526–533.

[47] J. Peng, C. Hou, L. Shen, Numerical analysis of corner-supported composite modular buildings under wind actions, J. Constr. Steel Res. 187 (September) (2021), 106942.

[48] A. Fathieh, O. Mercan, Seismic evaluation of modular steel buildings, Eng. Struct. 122 (2016) 83–92.

[49] C. Fang, Q. Zhong, W. Wang, S. Hu, C. Qiu, Peak and residual responses of steel moment-resisting and braced frames under pulse-like near-fault earthquakes, Eng. Struct. 177 (2018) 579–597.

[50] A. Memari, "Identification of Structural Issues in Design and Construction of Multi- Story Modular Buildings".

[51] A. Arias, Measure of Earthquake Intensity, 1970.

[52] Y. Park, A.H.S. Ang, Y.K. Wen, Seismic damage analysis of reinforced concrete buildings, J. Struct. Eng. 111 (4) (Apr. 1985) 740–757.

[53] E. Cosenza, G. Manfredi, The improvement of the seismic-resistant design for existing and new structures using damage criteria, Seism. Des. Methodol. next Gener. codes (1997) 119–130.

[54] J.W. Reed, R.P. Kassawara, A criterion for determining exceedance of the operating basis earthquake, Nucl. Eng. Des. 123 (2–3) (Oct. 1990) 387–396.

[55] P. Fajfar, T. Vidic, M. Fischinger, A measure of earthquake motion capacity to damage medium-period structures, Soil Dynam. Earthq. Eng. 9 (5) (Sep. 1990) 236–242.

[56] G.W. Housner, Behavior of structures during earthquakes, J. Eng. Mech. Div. 86 (4) (1960) 109–129.

[57] S.K. Sarma, K.S. Yang, An evaluation of strong motion records and a new parameterA95, Earthq. Eng. Struct. Dynam. 15 (1) (Jan. 1987) 119–132.

[58] O.W. Nuttli, The Relation of Sustained Maximum Ground Acceleration and Velocity to Earthquake Intensity and Magnitude, Miscellane, US Army Engineer Waterways Experiment Station, 1979. Report 16.

[59] J.L. von Thun, L.H. Roehm, G.A. Scott, J.A. Wilson, Earthquake Ground Motions for Design and Analysis of Dams, Geotech. Spec. Publ., no. n, 1988, pp. 463–481.

[60] S.L. Kramer, Geotechnical Earthquake Engineering, Pearson Education India, 1996.

[61] E.M. Rathje, N.A. Abrahamson, J.D. Bray, Simplified frequency content estimates of earthquake ground motions, J. Geotech. geoenvironmental Eng. 124 (2) (1998) 150–159.

[62] P.P. Cordova, G.G. Deierlein, S.S.F. Mehanny, C.A. Cornell, Development of a two-parameter seismic intensity measure and probabilistic assessment procedure, in: The Second US-Japan Workshop on Performance-Based Earthquake Engineering Methodology for Reinforced Concrete Building Structures, 2000, pp. 187–206.

[63] Y. Zhou, N. Su, X. Lu, An elastic spectral value-based intensity measure for the incremental dynamic analysis of tall buildings, in: Proc. 5th Kwang-Hua Forum on Innovations and Implementations in Earthquake Engineering Research, 2012. Shanghai, China, 2012.

[64] P. Tothong, N. Luco, Probabilistic seismic demand analysis using advanced ground motion intensity measures, Earthq. Eng. Struct. Dynam. 36 (13) (2007) 1837–1860.

[65] A. Ansi, ANSI/AISC 360-10. Specification for Structural Steel Buildings, American Institute of Steel Construction," *Inc. Chicago*, 2010.

[66] P.-C. Hsiao, Seismic Performance Evaluation of Concentrically Braced Frames, University of Washington, 2012.

[67] J.W. Baker, C.A. Cornell, Vector-valued intensity measures for pulse-like near-fault ground motions, Eng. Struct. 30 (4) (2008) 1048–1057.

[68] V. Sharma, M.K. Shrimali, S.D. Bharti, T.K. Datta, Seismic fragility evaluation of semi-rigid frames subjected to near-field earthquakes, J. Constr. Steel Res. 176 (2021), 106384.

[69] A. Emami Koupaei, H. Saffari, R. Rasti, Investigating the effect of earthquake duration on concrete structures by analyzing the frequency content of acceleration time history, J. Rehabil. Civ. Eng. 9 (2) (2021) 21–40.

[70] F. Jalayer, C.A. Cornell, A Technical Framework for Probability-Based Demand and Capacity Factor (DCFD) Seismic Formats, RMS, 2003.

[71] N. Shome, Probabilistic Seismic Demand Analysis of Nonlinear Structures, Stanford University, 1999.

[72] S.G. Gavabar, M. Alembagheri, Structural demand hazard analysis of jointed gravity dam in view of earthquake uncertainty, KSCE J. Civ. Eng. 22 (10) (2018) 3972–3979.

[73] M. Yakhchalian, M. Yakhchalian, M. Yakhchalian, Reliable fragility functions for seismic collapse assessment of reinforced concrete special moment resisting frame structures under near-fault ground motions, Struct. Des. Tall Special Build. 28 (9) (2019) e1608.

[74] R. Bhasker, A. Menon, Characterization of ground motion intensity for the seismic fragility assessment of plan-irregular RC buildings, Structures 27 (2020) 1763–1776.

[75] K. Kostinakis, A. Athanatopoulou, K. Morfidis, Correlation between ground motion intensity measures and seismic damage of 3D R/C buildings, Eng. Struct. 82 (2015) 151–167.